# *Equilibration of Tyrosyl Radicals (Y[• over 356], Y[• over 731], Y[• over 730]) in the Radical Propagation Pathway of the Escherichia coli Class Ia Ribonucleotide Reductase*



**Citation:** Yokoyama, Kenichi, Albert A. Smith, Bjorn Corzilius, Robert G. Griffin, and JoAnne Stubbe. "Equilibration of Tyrosyl Radicals (Y356•, Y731•, Y730•) in the Radical Propagation Pathway of the Escherichia coli Class Ia Ribonucleotide Reductase." Journal of the American Chemical Society 133, no. 45 (November 16, 2011): 18420-18432.

**As Published:** http://dx.doi.org/10.1021/ja207455k

**Publisher:** American Chemical Society (ACS)

**Persistent URL:** http://hdl.handle.net/1721.1/82079

**Version:** Author's final manuscript: final author's manuscript post peer review, without publisher's formatting or copy editing

Published in final edited form as:
*J Am Chem Soc*. 2011 November 16; 133(45): 18420–18432. doi:10.1021/ja207455k.

# Equilibration of tyrosyl radicals ($Y_{356}$•, $Y_{731}$•, $Y_{730}$•) in the radical propagation pathway of the *E. coli* class Ia ribonucleotide reductase

**Kenichi Yokoyama**[†], **Albert A. Smith**[†,#], **Björn Corzilius**[†,#], **Robert G. Griffin**[†,#], and **JoAnne Stubbe**[†,‡,*]

[†]Department of Chemistry, Massachusetts Institute of Technology, 77 Massachusetts Avenue, Cambridge, MA 02139–4307

[‡]Department of Biology, Massachusetts Institute of Technology, 77 Massachusetts Avenue, Cambridge, MA 02139–4307

[#]Francis Bitter Magnet Laboratory, Massachusetts Institute of Technology, 77 Massachusetts Avenue, Cambridge, MA 02139–4307

## Abstract

*Escherichia coli* ribonucleotide reductase is an α2β2 complex that catalyzes the conversion of nucleotides to deoxynucleotides using a diferric-tyrosyl radical ($Y_{122}$•) cofactor in β2 to initiate catalysis in α2. Each turnover requires reversible long-range proton-coupled electron transfer (PCET) over 35 Å between the two subunits by a specific pathway ($Y_{122}$• ⇆ [$W_{48}$?] ⇆ $Y_{356}$ within β to $Y_{731}$ ⇆ $Y_{730}$ ⇆ $C_{439}$ within α). Previously, we reported that a β2 mutant with 3-nitrotyrosyl radical ($NO_2Y$•, 1.2 radicals/β2) in place of $Y_{122}$• in the presence of α2, CDP and ATP catalyzes formation of 0.6 equiv dCDP and accumulates 0.6 equiv of a new Y• proposed to be located on $Y_{356}$ in β2. We now report three independent methods that establish that $Y_{356}$ is the predominant location (85 – 90%) of the radical with the remaining 10 – 15% delocalized onto $Y_{731}$ and $Y_{730}$ in α2. Pulsed electron-electron double resonance spectroscopy on samples prepared by rapid freeze quench (RFQ) methods identified three distances: 30 ± 0.4 Å (88 ± 3%), 33 ± 0.4 Å and 38 ± 0.5 Å (12 ± 3%) indicative of $NO_2Y_{122}$•-$Y_{356}$•, $NO_2Y_{122}$•- $NO_2Y_{122}$•, and $NO_2Y_{122}$•-$Y_{731(730)}$•, respectively. Radical distribution in α2 was supported by RFQ EPR studies using $Y_{731}$(3,5-$F_2$Y) or $Y_{730}$(3,5-$F_2$Y)-α2 which revealed $F_2$Y•, and by studies using globally incorporated [β-$^2H_2$]Y-α2 and analysis using parameters obtained from 140 GHz EPR spectroscopy. The amount of Y• delocalized in α2 from these two studies varied from 6 to 15%. The studies together give the first insight into the relative redox potentials of the three transient Y•s in the PCET pathway and their conformations.

## Introduction

Class Ia ribonucleotide reductases (RNRs) catalyze the reduction of nucleoside 5´-diphosphates (NDPs) to 2´-deoxynucleoside 5´-diphosphates (dNDPs) in all organisms and thereby provide the monomeric building blocks required for DNA replication and repair and

Corresponding Author: stubbe@mit.edu.

**SUPPORTING INFORMATION**. LC-MS analysis of peptides from tryptic digestion of wt-α2 and [β-$^2H_2$]Y-α2; effects of sample preparation conditions on the PELDOR spectra; CW-EPR spectra of the reactions with [$NO_2Y_{122}$•]-β2/wt-α2/ATP/CDP; time course of $NO_2Y$• reduction and the pathway radical formation; definition of θ; quantitation of [β-$^2H_2$]Y• at 12, 24, and 60 ms at 25 °C; EPR spectral simulation of [β-$^2H_2$]Y•; an Arrhenius plot of the $NO_2Y$• reduction in the [$NO_2Y_{122}$•]-β2/wt- α2/ATP/CDP reaction; and summary of dihedral angles (θ) for the Ys in α2. This material is available free of charge via the Internet at http://pubs.acs.org.

control their relative ratios, essential for the fidelity of these processes[1,2]. *E. coli* RNR consists of two homodimeric subunits, α2 and β2. α2 houses the binding sites for substrates (S: UDP, CDP, ADP, or GDP) and effectors (E: ATP, dATP, TTP, or dGTP) that control the specificity and rate of nucleotide reduction. β2 harbors the diferric tyrosyl radical ($Y_{122}$•) cofactor, which reversibly and transiently oxidizes $C_{439}$ in the active site of α2, which then initiates nucleotide reduction. A docking model of the active α2β2 complex was first proposed by Uhlin and Eklund[3] using the shape complementarity of the individual crystal structures of each subunit, in which $Y_{122}$ in β2 is >35 Å from the $C_{439}$ in α2. This distance is too large for the oxidation to occur by electron tunneling, given the enzyme's turnover number of 2–10 $s^{-1}$ and thus these observations led to the proposal[3,4] that the radical propagation proceeds by a hopping mechanism through conserved aromatic amino acid residues located in α2 and β2 (Figure 1). Our recent studies[5] showed that a new Y• is formed when a mutant β2 with a 3-nitrotyrosyl radical ($NO_2Y$•) in place of $Y_{122}$• ([$NO_2Y_{122}$•]-β2) is incubated with α2, CDP and ATP. This paper reports the use of three independent methods, pulsed-electron electron double resonance (PELDOR) spectroscopy, site-specific incorporation of 3,5-$F_2Y$ ($F_2Y$) in place of $Y_{731}$- or $Y_{730}$-α2, and global incorporation of [β-$^2H_2$]Y-α2, to establish that the newly trapped Y• is predominantly located at $Y_{356}$ in β2 (~87%) and is also delocalized into $Y_{731}$ and $Y_{730}$ in α2 (~13%).

Figure 1 shows our current proposal[6] for the radical propagation steps in RNR where the oxidation of $C_{439}$ by $Y_{122}$• occurs in multiple steps involving orthogonal or co-linear proton coupled electron transfer (PCET) (Figure 1). Mechanistic studies of this process were initially hampered by the rate-limiting protein conformational change(s) (2–10 $s^{-1}$) triggered by substrate and effector binding to α2 that precedes the radical propagation process and consequently masks all the subsequent steps.[7] While initial mutagenesis studies suggested the importance of the residues in the pathway[8,9], the mutant's inactivity precluded mechanistic studies. Thus, to investigate the mechanism, our laboratory has utilized Y analogs with different redox potentials and/or phenolic p$K_a$s, site-specifically replacing the Ys in the pathway. The pathway dependence of radical propagation and the redox reactivity of the $Y_{356}$, $Y_{731}$ and $Y_{730}$ were established, for example, using 3-hydroxytyrosine (DOPA)[10] or 3-aminotyrosine (3-$NH_2Y$)[11], both of which function as radical traps.

Recently, we reported the results of our studies[5] of the reaction of [$NO_2Y$•$_{122}$]-β2 (1.2 /β2) with α2/ATP/CDP using pre-steady state methods including stopped flow (SF) absorption spectroscopy, rapid freeze quench (RFQ) EPR spectroscopy and rapid chemical quench (RCQ) technology (Figure 2). Kinetic analysis revealed that 0.6 equiv of $NO_2Y$• was rapidly reduced to 0.6 equiv of $NO_2Y$ phenolate, with rate constants of ~300 and ~100 $s^{-1}$ and that 0.6 equiv of dCDP and a new radical were produced with similar kinetics. These rate constants are significantly faster than the conformationally gated catalysis by wt RNR[7], which occurs at 2–10 $s^{-1}$. The observed nitrophenolate and its stoichiometry indicate that in the reduction of $NO_2Y_{122}$• the electron transfer is uncoupled from the proton transfer and the fast rates of its formation indicate that protein conformational gating is also altered. The unusual stoichiometry is indicative of half-site reactivity inherent to the system[10–13]. Additional studies of $NO_2Y$•$_{122}$-β2 with redox inactive α2 mutants in the pathway ($C_{439}$S-α2, $Y_{730}$F-α2 and $Y_{731}$F-α2) led to the proposal that the new radical was located on $Y_{356}$ in β2[5].

The half-sites reactivity observed with the [$NO_2Y_{122}$•]-β2α2 experiments, suggested that pulsed electron electron double resonance (PELDOR) spectroscopy would provide an excellent tool to determine the location of the new Y•. PELDOR is a pulsed EPR method that allows measurement of weak dipolar interactions between two paramagnetic sites separated by 20 to 80 Å[14]. The measurements are possible due to the apparent half-sites reactivity of the active complex of RNR. Specifically, when a DOPA or 3-$NH_2Y$ is site-

specifically incorporated in place of a pathway Y residue, S/E binding to the complex triggers $Y_{122}$• reduction in one α/β pair and formation of DOPA• or $NH_2Y$• within the same pair[15]. However, the second α/β pair is unable to trigger a similar reaction, due to a loss of the appropriate signal from the first pair, and thus $Y_{122}$• in this second pair remains unchanged. Thus, the distance measured is between the $Y_{122}$• on one α/β pair and the new radical on the second α/β pair across the subunit interface as shown in Figure 3. This method allowed measurement of five distances within the "active" α2β2 complex, which are within error of those predicted from the docking model[12,15,16].

In the present report we describe the use of PELDOR spectroscopy to establish the location of the new Y• generated from incubation of [$NO_2Y_{122}$•]-β2/α2/CDP and ATP. Unexpectedly the data suggested that the new Y• is not uniquely located in β2, but equilibrates onto one or both of the two pathway tyrosines in α2. To provide additional support for the interpretation of the PELDOR experiments, α2 with 3,5-difluorotyrosine ($F_2Y$) site-specifically incorporated at 731- or 730-α2, and α2 globally labeled with [β-$^2H_2$]Y were examined by RFQ EPR spectroscopy and the amount of Y• located in α2 quantitated. The results together suggest that the Y• is primarily localized (~87%) at $Y_{356}$-β2 with ~13% equally distributed between $Y_{731}$ and $Y_{730}$ in α2. Using the [β-$^2H_2$]Y-α2 results and data obtained from high field EPR spectra of the Y•s generated with wt-α2 and $Y_{731}$F-α2, analysis of the temperature dependent shift of the equilibrium between the radicals in β2 and α2 suggested that the redox potential of $Y_{356}$-β2 is ~100 mV lower than that at $Y_{731}$- and $Y_{730}$-α2. Furthermore, the studies of the trapped Y•s by 9 and 140 GHz EPR spectroscopy have provided information on the conformation and electrostatic environment of the pathway Y residues in the active α2β2 complex.

## Materials and Methods

[β-$^2H_2$]Y was from Cambridge Isotope Laboratory (Andover, MA). EPR tubes for 9-GHz spectroscopy (quartz, O.D. 4 mm, I.D. 3.2 mm) were from Wilmad Labglass (Vineland, NJ). EPR tubes for 140-GHz spectroscopy (silica, O.D. 0.55 mm, I.D. 0.40 mm) were from Optic Fiber Center Inc. (New Bedford, MA). 2,6-Difluorophenol and 3-nitrotyrosine ($NO_2Y$) were purchased from Sigma-Aldrich. Isopropyl-β-D-thiogalactopyranoside (IPTG) and dithiothreitol (DTT) were from Promega. 3,5-Difluorotyrosine (3,5-$F_2Y$) was synthesized from 2,6-fluorophenol, sodium pyruvate and ammonium acetate using tyrosine phenol lyase as described previously[17]. The purification of wt-α2[18] (2200–2700 nmol/min/mg), $Y_{731}$F-α2[18], [3,5-$F_2Y_{730}$]-α2[19] (1200–1300 nmol/min/mg at pH 7.6), [3,5-$F_2Y_{731}$]-α2[19] (1300–1500 nmol/min/mg at pH 7.6) and [$NO_2Y_{122}$]-β2[20], have previously been described. The concentrations of wt and mutant α2s were determined using $\varepsilon_{280nm}$ = 189 $mM^{-1}$ $cm^{-1}$.[21] The concentrations of [$NO_2Y_{122}$]-β2 and apo-[$NO_2Y_{122}$]-β2 were determined using $\varepsilon_{280nm}$ = 131 and 120 $mM^{-1}$ $cm^{-1}$, respectively[22].

### Determination of the distance between Y• and $NO_2Y$• by PELDOR spectroscopy

Samples for the PELDOR experiments were prepared by the RFQ method as described previously[5] using an Update Instruments 1019 Syringe Ram Unit equipped with three syringes and a Model 715 Syringe Ram Controller. Fe(II) pre-loaded [$NO_2Y_{122}$]-β2 (300 μM, 5 Fe(II)/β2, 150 μL) in anaerobic buffer A [50 mM HEPES (pH 7.6) containing 5% (w/v) glycerol] from one syringe was mixed with an equal volume of buffer A with $O_2$ (1.3 mM, saturated at 25 °C) and CDP (3 mM) from another syringe and aged for 0.17 s at 25 °C. This solution (300 μL) was then mixed with 150 μL of a solution containing wt- or $Y_{731}$F-α2 (300 μM), ATP (9 mM), EDTA (3 mM) and $MgSO_4$ (45 mM) in buffer A from the third syringe. The final reaction mixture contained 100 μM [$NO_2Y_{122}$]-β2, 100 μM α2, 3 mM ATP, 1 mM CDP, 1 mM EDTA, and 15 mM $MgSO_4$ in buffer A. The reaction mixture was

incubated for 8 – 570 ms, sprayed into a funnel containing liquid isopentane at −143 ± 3 °C, and then packed into an EPR tube.

PELDOR spectra were recorded at 5 K using a Bruker ELEXSYS E580 X-band spectrometer and a dead-time free four-pulse DEER sequence[23]. π/2 and π-pulses on the detection frequency were 16 and 32 ns, respectively; the π pulse on the pump frequency was typically 32 ns; τ (spacing between π/2 and π-pulse) = 128 ns; $T$ = 5 K; 24 – 48 h acquisition time. The data were analyzed using DeerAnalysis 2009 software[24]. To extract the modulation frequency, a monoexponential decay function was fit and subtracted from each curve. The resulting oscillation curve was analyzed using the Tikhonov regularization procedure[25]. The regularization parameter, α term, was determined by the L-curve criterion[24,25].

### Determination of EPR spectrum of $Y_{356}$• at 140 GHz

All reactions were performed by hand-mixing at room temperature (20 ± 2 °C). Apo-[$NO_2Y_{122}$]-β2 (0.4 mM) in $O_2$ saturated 50 mM HEPES pH 7.6 (10 μL) was mixed with 2 μL of 10 mM Fe(II) in 5 mM $HNO_3$ and incubated for ~5 s, and then mixed with an equal volume of 0.34 mM wt-α2 or $Y_{731}$F-α2, 6 mM ATP and 2 mM CDP in 2x assay buffer. The final solution contained 170 μM [$NO_2Y_{122}$] -β2, 170 μM wt-α2 or $Y_{731}$F-α2, 3 mM ATP, 1 mM CDP in assay buffer. The sample was drawn into an EPR sample tube by capillary action to a height of > 2 mm, and loaded into the side-coupled $TE_{011}$ cylindrical resonator of the EPR probe, which was then inserted in a cryostat maintained at 70 K by liquid He. The sample was frozen in the cryostat within 15 s of the second mixing by a stream of cold He gas. The 140 GHz pulsed EPR spectra were recorded at 70 K on a home-built spectrometer[26,27] using a π/2-π spin echo sequence[28] with typical π/2 and π pulse lengths of 32 ns and 64 ns, respectively, and τ, the time between π/2 and π–pulses, of 200 ns.

### Investigation of Y• distribution in α2 using [3,5-$F_2Y_{731}$]-α2 and [3,5-$F_2Y_{730}$]-α2

The reactions were performed at 25 °C as described above for the PELDOR sample preparation except that [$NO_2Y_{122}$•]-β2 (30 μM) and [3,5-$F_2Y_{731}$]-α2 or [3,5-$F_2Y_{730}$]-α2 (30 μM) were used. The reactions were freeze-quenched at 60 ms and packed into EPR tubes. CW-EPR spectra were recorded on a Bruker ESP 300 X-band spectrometer equipped with a quartz finger dewar filled with liquid $N_2$. EPR parameters were: microwave frequency = 9.34 GHz, power = 30 μW, modulation amplitude = 1.5 G, modulation frequency = 100 kHz, time constant = 5.12 ms, scan time = 41.9 s, conversion time = 20.48 ms. EPR spin quantitation was carried out using Cu(II)$SO_4$ as a standard.[29] All EPR spectral simulations were carried out using the EasySpin software[30].

### Expression and purification of [β-$^2H_2$]Y-α2

*E. coli* DH10B cells transformed with a pTrc-*nrdA*[11] were grown at 37 °C in a previously described amino acid (Glu, Gln, Asp, Asn, Lys, Val, Arg, Leu, His, Ile, Ala, Pro, Trp, Gly, Met, Thr, Ser, 0.2 g/L) enriched GMML[20] supplemented with 1 mM [β-$^2H_2$]Y and 100 mg/L ampicillin. α2 expression was induced at $OD_{600}$ = ~ 0.8 by an addition of 1 mM IPTG. The growth was continued for another 4 h and the cells were harvested by centrifugation (4,000 × $g$, 10 min), yielding 5 g/L cell paste. [β-$^2H_2$]Y-α2 was then purified using a previously described procedure[18] with a yield of ~ 5 mg/g of cell paste. To determine the extent of [β-$^2H_2$]Y incorporation, the purified protein was digested by L-1-tosylamido-2-phenylethyl chloromethyl ketone treated Porcin trypsin (Sigma) and the peptides analyzed by LC-MS at the Koch Institute at MIT (see Supporting Methods and Figure S1 for details). In the non-labeled wt-α2 sample, a doubly charged peptide with $m/z$ 529.76 ± 0.03 was eluted at 11–12 min (Figure S1A), which agrees with $m/z$ of 529.77 for an expected tryptic peptide fragment (TLYYQNTR) containing $Y_{731}$- and $Y_{730}$-α2. The peptide sequence was

further confirmed by a tandem MS. In the [β-$^2H_2$]Y-α2 sample, a peptide with *m/z* 531.77 ± 0.05 along with a small signal with *m/z* of 529.77 were observed at the same retention time (11 – 12 min). Based on the relative intensities of these peaks in the [β-$^2H_2$]Y-α2 sample, the [β-$^2H_2$]Y incorporation was estimated to be > 92%.

### Investigation of the Y• distribution in α2 using [β-$^2H_2$]Y-α2

The reactions were carried out as described above for the PELDOR sample preparation at 25 °C except that [$NO_2Y_{122}$•]-β2 (30 μM) and [β-$^2H_2$]Y-α2 (30 μM) were used. The reactions were -freeze-quenched at 12, 24, 60 or 115 ms, and packed into EPR tubes. The CW-EPR spectra were recorded at 77 K and 9 GHz as described above. The amount of [β-$^2H_2$]Y• was quantitated as described in the Results. The EPR spectral simulations in the analysis were carried out using EasySpin software[30].

### Investigation of the temperature dependent distribution of the Y•s in α2 using [β-$^2H_2$]Y-α2

The reactions were carried out at 5, 15, 25 or 37 °C as described above for the PELDOR sample with the following modifications. Fe(II) pre-loaded [$NO_2Y_{122}$]-β2 (90 μM, 5 Fe(II)/β2, 150 μL) in anaerobic buffer A from one syringe was mixed with an equal volume of buffer A with $O_2$ (2.0, 1.6, 1.3 and 1.0 mM at 5, 15, 25 and 37 °C, respectively) and CDP (3 mM) from the second syringe and aged for 2, 0.2, 0.16, and 0.06 sec for the reactions at 5, 15, 25 and 37 °C, respectively. This solution (300 μL) was then mixed with 150 μL of a solution containing [β-$^2H_2$]Y-α2 or α2 (90 μM), ATP (9 mM), EDTA (3 mM), and $MgSO_4$ (45 mM) in buffer A from the third syringe. The final reaction mixture contained 30 μM [$NO_2Y_{122}$]-β2, 30 μM α2, 3 mM ATP, 1 mM CDP, 1 mM EDTA, and 15 mM $MgSO_4$ in buffer A. The reaction was incubated for 12, 24, 60 or 115 ms at 5, 15, 25 and 37 °C, respectively, sprayed into a funnel containing liquid isopentane at −143 ± 3 °C, and then packed into an EPR tube. The CW-EPR spectra were recorded at 77 K and 9 GHz, and analyzed as described above. The redox potential difference ($\Delta E°$) between $Y_{356}$-β2 and $Y_{731/730}$-α2 was determined from the observed amounts of [β-$^2H_2$]Y• using Eq. 1.

$$\mathrm{Log}([\beta\text{–}^2\mathrm{H}_2\text{–}\mathrm{Y}\bullet]/[\mathrm{Y}_{356}\bullet]) = (\Delta E^\circ \times \mathrm{F}/\mathrm{R}) \times (1/\mathrm{T}) \qquad \text{(Eq. 1)}$$

where F is the Faraday constant, R is the ideal gas constant, and T is the temperature in K. Details of the analysis, including the method of [β-$^2H_2$]Y• quantitation, are described in the Results.

## Results

### Optimization of sample preparation for PELDOR experiments

Our previous PELDOR experiments with DOPA•[15] and $NH_2Y$• (E. C. Minnihan and J. Stubbe unpublished results) generated at 356 in β2 in the reaction with CDP/ATP/α2 gave rise to the diagonal distance from $Y_{122}$• of 30 Å (Figure 3) in both cases. These results suggest that the PELDOR method would provide evidence for the location of the new Y•, generated when [$NO_2Y_{122}$•]-β2 is incubated with α2, CDP, and ATP. Optimization was required for the sample preparation to obtain reproducible, analyzable spectra with good ratio of signal to noise (S/N). An important variable was the method of freezing. Previously, all of our experiments were carried out with “hand-quenching” of samples in liquid nitrogen[12,15,16], that is, slow freezing. However in the current experiments the new radical(s) is (are) generated on a ms time scale requiring RFQ methods to trap them. Thus, we compared the results of the hand quench (red trace) and RFQ methods (blue trace) as shown in Figure S2A. In both sets of samples the concentration of glycerol was 5%. Subtraction of the monoexponential echo decay function from the observed spectra and

fitting by the Tikhonov regularization procedure[25] gave the results shown in Figure S2B. The modulations were markedly improved by the RFQ method or by addition of glycerol (Figure S2A yellow trace) to the hand quenched sample. This observation is consistent with previous studies that have established that the RFQ method minimizes protein aggregation problems[31]. A second variable is the spin/protein concentrations that were varied from 50 to 200 μM (total radical). The results are shown in Figure S2C. One hundred μM was chosen to minimize intermolecular dipolar couplings and retain excellent S/N (Figure S2D). Finally, the glycerol concentration was optimized. Previously, the effects of glycerol concentrations (0 – 40%) on hand quenched samples were investigated to measure Y•-Y• distances in *E. coli*[16] and mouse[32] β2, in which some glycerol (5%) was required to prolong the $T_2$ spin relaxation, while higher concentrations (10 – 40%) slowed $T_1$ requiring longer data acquisition times.[32] Similar effects were observed in the current study. In addition, the rate constant for the pathway Y• formation slowed down at glycerol concentrations higher than 10% (w/v), and the RFQ sample packing became very difficult due to the stickiness of the frozen solution at glycerol concentrations of ~30%. Thus, all samples for PELDOR measurements were prepared by the RFQ method with the protein (spin) concentration of 0.1 mM and glycerol concentration of 5%.

## Investigation of the location of pathway Y•s by PELDOR spectroscopy

The X-band (9 GHz) spin-echo detected absorption spectrum of the reaction between [$NO_2Y_{122}$•]-β2 with wt-α2/CDP/ATP with RFQ at 24 ms is shown in Figure 4 (black trace at 5 K and blue trace at 80 K). The visible doublet spectra arise from the hyperfine coupling (hfc) to one of the two β methylene protons (β-$^1$Hs) of Y or $NO_2Y$. The absorption EPR spectrum of the same sample at 80 K reveals only the new Y• (blue trace) as at this temperature the $NO_2Y$• is not visible due to its faster relaxation properties resulting from its proximity to the diferric cluster. The $NO_2Y$• (red trace) in β2 alone at 5 K is shown. A comparison of blue and red spectra reveal extensive overlap and thus the pump (P) and detection (D) frequencies for data acquisition were chosen to be at ~ peak maxima separated by 60 MHz[16]. Figure 5A shows the echo modulation trace observed for [$NO_2Y_{122}$•]-β2 alone after subtraction of a monoexponential signal decay function. The modulation frequency of this spectrum is indicative of the distance between two $NO_2Y_{122}$•s in β2 (Figure 3). Analysis of this trace using the distance-domain Tikhonov regularization procedure[25] resulted in the distance distribution profile shown in Figure 5B and a distance at 33.1 ± 0.4 Å. The error is based on the peak width at half height from three different sample preparations. Similar experiments with RFQ prepared wt-β2 samples with 5% glycerol gave improved fits with the distance at 33.2 ± 0.4 Å (Figure S2B). The poorer fit of the data with [$NO_2Y_{122}$•]-β2 alone relative to wt-β2 alone may be associated with the presence of excess Fe(III) resulting from the in vitro cluster assembly of [$NO_2Y_{122}$•]-β2, which is not present in wt-β2 assembled in vivo. The observed distance is consistent with the distance between the center of the aromatic rings of two $NO_2Y_{122}$s in the β2 dimer observed in the crystal structure of this mutant (32.8 Å)[5] and the $Y_{122}$•-$Y_{122}$• distance in wt-β2 previously determined by PELDOR (33.1 ± 0.2 Å)[16].

To measure the distance between the trapped Y• and $NO_2Y_{122}$•, the reaction with [$NO_2Y_{122}$•]-β2/wt-α2/ATP/CDP was freeze-quenched at 8 or 24 ms, where 21 ± 3% and 34 ± 4% of $NO_2Y$• was converted into the pathway Y•, respectively, determined by X-band CW-EPR spectroscopy (Figure S3). The observed echo modulation frequency exhibited time dependent changes from 8 to 24 ms (compare Figures 5C and 5E), indicating a transformation of $NO_2Y_{122}$• to the new radical. The distance distribution profiles shown in Figures 5D, and 5F reveal disappearance of the signal at 33 Å, the $NO_2Y_{122}$•-$NO_2Y_{122}$• distance, and appearance of two new features at 30 and 38 Å. The distance of 30.0 ± 0.4 Å is within the error of the distance previously observed for DOPA• at 356-β2 (30.6 ± 0.5 Å)[15]

and that recently measured for $NH_2Y$• at 356-β2 (30.2 ± 1.6 Å, E. C. Minnihan and J. Stubbe unpublished results) and is consistent with our previous assignment of the predominant species as $Y_{356}$•.

The unexpected small signal at 38 Å (Figure 5D and 5F) was observed in 10 different sample preparations quenched at 8, 24, 120 or 570 ms. The distance is close to those previously observed when [$NH_2Y_{731}$]-α2 and [$NH_2Y_{730}$]-α2 were used to generate $NH_2Y$• at 731-α2 (38.1 ± 1.2 Å) and 730-α2 (38.7 ± 1.8 Å)[15], respectively. The peak area associated with this feature ranged from 8 – 15% of the 30 Å feature. As one test of the "reality" of the 38 Å feature, the Tikhonov regularization analysis was carried out by limiting the distance distribution range from 20 – 36 Å. The results of these analyses are shown in Figures 5C and 5E (green traces), which are very similar to the analyses with the full distance range (20 – 50 Å). Thus, the analysis itself cannot establish the reality of the 38 Å peak. However, the peak was reproducibly observed in all samples regardless of the choice of the Tikhonov regularization parameter, α, or the position of the background fitting, suggesting that the peak is not an artifact of the data analysis.

If the 38 Å feature is associated with Y•(s) in α2, the 38 Å distance would not be observable in a PELDOR experiment using $Y_{731}$F-α2 in place of wt- α2, which would localize the radical at $Y_{356}$-β2. It is important to point out, however, that the $Y_{356}$• observed in this mutant reaction is generated in the forward radical propagation and not the back radical propagation as in the wt-α2 reaction. The reaction was quenched at 8 ms and 25 ± 2% of the total radical was trapped as the pathway Y•. The PELDOR experiments and analyses on four independently prepared samples quenched at 8 or 24 ms revealed only two distances: 30 and 33 Å[33]. Although the fits are not as good as those for wt-α2 experiments (compare Figures 5C and 5E with 5G), they provide support for our proposal that the 38 Å distance observed in wt-α2 reactions is associated with Y•s at 731/730 in α2.

### High-field EPR (HF-EPR) of $Y_{356}$•

As described subsequently, further studies to obtain evidence for new radical delocalization in α2 required EPR spectral simulations. Thus the g-values and hfcs for the $Y_{356}$• were determined by simulation of EPR spectra at 9 and 140 GHz. As this is the first Y• observed on the pathway, determination of these parameters are important in understanding the protein environment, its H-bonding interactions and electrostatic environment, and the conformation of the $Y_{356}$-β2 in the active α2β2 complex. In addition, determination of the g-values and hfc parameters will also allow us to compare them with those measured for $NH_2Y_{356}$• and $DOPA_{356}$• and offer one method to evaluate the extent of the perturbations caused by the presence of an $NH_2$ or OH group at the ortho position to the phenol of these amino acids.

$Y_{356}$• was generated either with wt- or $Y_{731}$F-α2 and [$NO_2Y_{122}$•]-β2/CDP/ATP by hand mixing/freezing[5]. In the $Y_{731}$F-α2 case, only $Y_{356}$• is observable in addition to the $NO_2Y_{122}$•, while in the wt-α2 case, the trapped radical is composed of $Y_{356}$• and up to 15% of additional radical species. We have previously reported that the pulsed EPR method can filter the signal of radicals in α2[34] and at 356 in β2 (unpublished results) from that of $Y_{122}$• in β2, when the electron spin echo spectrum is recorded at 70 K. At this temperature and 140 GHz, we verified that the signal associated with $NO_2Y_{122}$•, adjacent to the diferric cluster, is not observable. The resulting absorption spectra for wt- or $Y_{731}$F-α2 were obtained and converted to the first derivative spectra as shown in Figures 6A and 6C, respectively. The corresponding 9 GHz CW-EPR spectra were also acquired by hand quenching and the $NO_2Y_{122}$• spectrum removed by subtraction[5] (Figures 6B and 6D).

Analysis of the spectra at these two frequencies required a simulation strategy in which the constraints posed by the spectra at the different frequencies were determined, as far as possible, and then combined to find a global solution. The simulation of the 9 GHz spectra was attempted first by assuming one large isotropic hfc for one of the β-$^1$Hs, a line broadening factor of 11 MHz associated with the unresolved hfcs, and anisotropic hfcs for the 3,5-$^1$Hs of the ring ([$A_{xx}$, $A_{yy}$, $A_{zz}$] = [27, 8, 19] MHz), almost invariable in Y•s observed in biological systems[35]. Because the X-band EPR spectra are rather insensitive to g-values, the values for $Y_{122}$• in wt-β2 (2.009, 2.0046, 2.0023) were initially used. The 140 GHz spectra were then simulated using the parameters obtained from the 9 GHz simulations. The deviation in the g-values was immediately observed, and the values were adjusted. The hfcs for β-$^1$H were also varied and line broadening factors associated with the width of Gaussian distribution of g-values (g strain) were introduced. The simulations were repeated between the spectra at 140 GHz and 9 GHz until the square deviations at both frequencies were minimized. The results of the final simulations are shown in Figure 6 (red), and the parameters summarized in Table 1. While the simulation reproduced the Y• spectrum from the experiments with the $Y_{731}$F-α2, the simulation of the wt-α2 reaction at 140 GHz did not reproduce the shoulder feature at 49800 – 49830 G suggesting the presence of an additional minor component(s). This deviation was not detectable at 9 GHz and thus the additional species likely has perturbed g-values with hfcs similar to the predominant species. The major species in the wt-α2 reaction has $g_{xx}$ value of 2.0063, distinct from the value of 2.0073 found in the $Y_{731}$F-α2 reaction (Table 1). $Y_{356}$• is the predominant species in both reactions based on the PELDOR data and other experiments described subsequently. The protein environments of the two radicals are identical except that the OH of $Y_{731}$ is replaced with a H in the mutant. The $g_{xx}$ values of Y•s in biology have been shown to be sensitive to their H-bonding/electrostatic environments with values varying between 2.006 – 2.009 with the smaller values associated with H bonding.[35–38] Thus the current observation is intriguing in terms of differences in H bonding.

## Probing radical distribution at 731 and 730-α2 using [3,5-$F_2Y_{731}$]- and [3,5-$F_2Y_{730}$]-α2 mutants

Two types of experiments were carried out to provide further support that the new radical is composed of three Y•s with ~10% delocalized at $Y_{731}$- and $Y_{730}$-α2. Detection of small amounts of Y• in α2 in the presence of $NO_2Y_{122}$• and $Y_{356}$• is challenging as the EPR spectra of all the species overlap (Figure 4). We have recently evolved a tRNA/tRNA synthetase pair that can site-specifically incorporate a series of $F_nY$ (n = 2 or 3) into either β2 or α2[19]. RNR with 3,5 $F_2Y$ for example in place of $Y_{122}$-β2, $Y_{731}$- or $Y_{730}$-α2 have been prepared. Our studies with 3-FY•[17] and 3,5 $F_2Y$•[19] at residue 122 in β2 reveal that these radicals exhibit characteristic splitting patterns with couplings of ~54 MHz associated with a β-$^1$H, similar to the hfc of a β-$^1$H in $Y_{122}$•. In addition, strong couplings of 150 – 180 MHz associated with the $^{19}$F nucleus are also readily detected in the low field and high field regions of the EPR spectrum, as they appear outside the contribution from the features associated with Y•s. Thus, 3,5 $F_2Y$• is detectable even in the presence of $NO_2Y$• and other pathway Y•s. 3,5-$F_2Y$ was chosen as a probe to look for radical delocalization in α2 because its redox potential is within ± 30 mV of that of Y between pH 6.5 and 8.0, if we assume that the p$K_a$ of this residue is not significantly perturbed in the protein environment[17]. Our previous studies using $NO_2Y$ as a reporter on p$K_a$ perturbation at 731 and 730 positions in α2 have shown this to be the case (p$K_a$ perturbation of ≤ 1.2 pH unit).[20]

The reactions of [$NO_2Y_{122}$•]-β2 with [3,5-$F_2Y_{731}$]-α2 or [3,5-$F_2Y_{730}$]-α2 in the presence of ATP and CDP were therefore carried out at 25 °C, pH 7.6, with rapid freeze quenching at 60 ms. If we assume that the kinetics of radical propagation with these mutants are similar to that with wt-α2, a reasonable assumption based on the measured specific activities of these

mutants (60 – 80% of wt-α2 at pH 7.6[19]), 50% of initial $NO_2Y$• should be reduced and a corresponding amount of pathway radicals should be formed (Figure S4). Figure 7 shows the EPR spectra of the quenched reactions with [3,5-$F_2Y_{731}$]-α2 or [3,5-$F_2Y_{730}$]-α2 after subtraction of the $NO_2Y$• spectrum (50% of the total radical). Immediately apparent are the characteristic features on the high- and low-field side of each spectrum, indicative of the hyperfine splitting associated with $^{19}$Fs and a β-$^1$H (see brackets in Figure 7). The feature indicated by * in Figure 7D is unidentified and is also observed in the reaction with wt-α2. Despite the overlap of most of the spectrum of each 3,5-$F_2Y$• with that of the predominant $Y_{356}$•, each $F_2Y$• spectrum was simulated to reproduce its low field and high field features. The g-values [($g_{xx}$, $g_{yy}$, $g_{zz}$) = (2.0063, 2.0044, 2.0022)] were chosen based on the HF-EPR spectra for the trapped Y• observed in wt-α2 (Figure 6A). Variation of the $g_{xx}$ values ranging from 2.0091 (wt-$Y_{122}$•) to 2.0063 in the simulation of the 9 GHz spectra showed minimal effect and can therefore be neglected. The hfcs for 2,6-$^1$Hs and for the second β-$^1$H are in general smaller than the intrinsic line width (17 MHz), and thus were not included specifically in the simulation. Thus the key variables in the simulations are the hfc associated with one of the β-$^1$Hs, assumed to be isotropic, and that with the $^{19}$F nucleus. The results of the simulations are shown in Figure 7 (red traces) and the hfcs are summarized in Table 1. The hfcs associated with $^{19}$Fs are 157 and 151 MHz for [3,5-$F_2Y_{731}$]-α2 and [3,5-$F_2Y_{730}$]-α2, respectively, similar to those previously reported for 3-$FY_{122}$•[17] and 3,5-$F_2Y_{122}$•[19]. The β-$^1$H hfcs are 40 ± 5 and 63 ± 6 MHz for [3,5-$F_2Y_{731}$]-α2 and [3,5-$F_2Y_{730}$]-α2, respectively.

The amount of 3,5-$F_2Y$• was approximated from the simulated spectrum. The signal heights of the doublet features in the simulated and experimental spectrum were adjusted (Figure 7B and 7D), and the double integrals of two spectra compared. This analysis contains significant error associated primarily with the line broadening factors (17 ± 4 MHz) used in the simulations, which affected the height of the doublet features. Nevertheless, the analyses of three independent experiments indicate that 3,5-$F_2Y_{731}$• and 3,5-$F_2Y_{730}$• accounted for 5 ± 3 and 9 ± 4% of the trapped pathway radicals, respectively. The sum of these values is similar to the intensity of the 38 Å peak (8 – 15%) observed in the PELDOR experiments. The observation of $F_2Y$• unambiguously establishes the presence of the radical in α2 at both pathway residues[39].

The hfc of β-$^1$H reports on different geometries of the tyrosyl side chain within the protein. The isotropic part ($A_{iso}$) of the hfc for one of the β-$^1$Hs not only depends on the spin density of the adjacent carbon of the ring system (C1), but in addition, there is a strong dependence on the geometry of the side chain according to $A_{iso} \approx (B_1 \times \rho^{\pi}_{C1} \times \cos^2 \theta)$, where $\rho^{\pi}_{C1}$ is the π-spin density at C1, θ (Figure S5) is the dihedral angle between the $C_\beta$-H bond and the $p_z$ orbital at C1, and $B_1$ is an empirical constant and assumed to be 162 MHz[40]. The $A_{iso}$ for one of the β-$^1$Hs of 3,5-$F_2Y_{730}$• is 63 MHz, while that for the other is not observable and is smaller than the intrinsic line width of ~17 MHz of the spectrum. Using this value, one can calculate θ = −70 ± 6° or +10 ± 5° ($\rho_{C1}$ = 0.41 ± 0.02), which is consistent with the conformation of $Y_{730}$-α2 (θ = −67 ± 4°) observed in the crystal structures of wt-[3,41] and mutant α2s[8,20,42].

A similar analysis for 3,5-$F_2Y_{731}$• allows calculation of θ = + 80 ± 3° or + 40 ± 3° ($\rho_{C1}$ = 0.42 ± 0.02). Two conformations have been reported for $Y_{731}$ in wt and mutant α2s. The one most frequently found and shown in most renditions of the structure has θ = + 3 ± 3° (Figure 8 blue structure)[3,41]. Recently, however, a second conformation has been reported in our $NH_2Y_{730}$-α2 crystal structure in one of the three subunits in the asymmetric unit. In this case, θ = +82° (Figure 8 green structure)[42]. The hfc of 3,5-$F_2Y_{731}$• is most consistent with the latter. This observation suggests that $Y_{731}$-α2 is flexible and may undergo

conformational changes upon complex formation with β2 to catalyze radical propagation. If this conformation is catalytically active, then it has interesting mechanistic implications.

### Probing radical distribution in α2 using [β-$^2H_2$]Y-α2

As the second approach to obtaining evidence for Y• distribution over multiple residues, α2 was prepared with [β-$^2H_2$]Y replacing all Ys. [β-$^2H_2$]Y was chosen based on the difference in gyromagnetic ratios of $^1H$ and $^2H$, which reduces the hfc associated with β-$^1H$ 6.5-fold and collapses the doublet feature of the Y• EPR signal into a broad singlet. Thus, [β-$^2H_2$]Y• can be detected as a change in the EPR line shape even though it contributes to only 10 – 15% of the new Y•.

[β-$^2H_2$]Y was globally incorporated by overexpression of wt-α2 in a defined medium containing [β-$^2H_2$]Y instead of Y. [β-$^2H_2$]Y-α2 was purified to homogeneity and had a specific activity of 2300 nmol/min/mg, comparable to wt-α2. The extent of label incorporation was determined as > 92% by LC-MS analysis of peptides from trypsin digestion (see Supporting Methods and Figure S1 for details).

The kinetics of the reaction of [β-$^2H_2$]Y-α2 with [$NO_2Y_{122}$•]-β2/ATP/CDP were studied at 25 °C with quenching at 12 – 115 ms. Analysis of the EPR spectra involved subtraction of the $NO_2Y$• spectrum from the observed spectrum using the broad feature at the low field side of the $NO_2Y$• spectrum as described previously[5]. The amount of $NO_2Y$• reduced and new pathway radical formed was very similar to results previously reported with wt-α2 (Figure S4). The resulting spectrum of the pathway radicals quenched at 115 ms is shown in Figure 9A (red spectrum) and is distinct from that observed in the reaction with wt-α2 (gray spectrum). Similar spectra were observed at other quench times (Figure S6).

The amount of [β-$^2H_2$]Y• in α2 was quantitated by reproducing the observed EPR spectrum by varying the amount of $Y_{356}$• spectrum, from the EPR spectrum of Y• observed in the $Y_{731}$F-α2/[$NO_2Y_{122}$•]-β2/ATP/CDP reaction, and the amount [β-$^2H_2$]Y•$_{730/731}$ spectrum, from simulations described subsequently. The EPR spectrum of $Y_{356}$• was assumed to be identical to that observed in the RFQ experiment of the $Y_{731}$F-α2/[$NO_2Y_{122}$•]-β2/ATP/CDP reaction. Although our HF-EPR spectrum at 140 GHz revealed that the $Y_{731}$F mutation perturbs the $g_{xx}$-value of $Y_{356}$•, this spectral perturbation at 9 GHz is minimal (compare Figures 6B and 6D). The EPR spectrum of [β-$^2H_2$]Y• was simulated using the parameters in Table 1 obtained from the following analysis. The hfcs for β-$^2H$ of [β-$^2H_2$]Y• at 731- and 730-α2 were calculated to be 6 and 10 MHz, respectively, assuming that the hfcs simulated for 3,5-$F_2$Y•s are indicative of the Y• conformation in these positions. The simulations with hfcs within this range resulted in very similar spectra (Figure S7) and therefore, [β-$^2H_2$]Y• in α2 was simulated with an $A_{iso}$ of 8 MHz. The g-values in the simulations were [$g_{xx}$, $g_{yy}$, $g_{zz}$] = [2.0063, 2.0044, 2.0022] and their variation made little difference as described above for the simulation of 3,5-$F_2$Y•. The resulting simulated spectrum of [β-$^2H_2$]Y• was then combined with the $Y_{356}$• spectrum in appropriate ratios to reproduce the experimentally observed spectra (Figure 9B and Figure S6). For example, the sum of $Y_{356}$• spectrum (blue, 87%) and the simulated [β-$^2H_2$]Y• spectrum (pink, 13%) is shown in the black trace in Figure 9B and compared with the spectrum of the pathway radical observed in the reaction with [β-$^2H_2$]Y-α2 freeze-quenched at 115 ms (red trace). The ratio of the $Y_{356}$• and simulated [β-$^2H_2$]Y• spectra was optimized by minimizing the root mean square deviation of the black trace from the red trace.

The EPR spectra of pathway Y• at the other time points (12, 24, 60 and 115 ms) were analyzed in a similar manner (Figure S6). The pathway Y• was 35 ± 3, 41 ± 2, 49 ± 2 and 50 ± 2% of total radical and the amounts of [β-$^2H_2$]Y• were 15 ± 2, 13 ± 2, 13 ± 2, and 13 ± 1% for 12, 24, 60 and 115 ms, respectively, from three independently prepared samples. The

errors are associated mainly with the subtraction of the $NO_2Y_{122}$• spectrum. These observations, with the caveats associated with the assumptions described above, suggest that the amounts of [β-$^2H_2$]Y•s in α2 are similar over the time course and that 13–15% of total Y• is distributed in α2 and are in equilibrium with the $Y_{356}$• in β2.

### Temperature dependent equilibration between $Y_{356}$• and [β-$^2H_2$]Y• in α2

If $Y_{356}$•-β2, $Y_{731}$•- and $Y_{730}$•-α2 are in equilibrium, the ratio of $Y_{356}$• vs [β-$^2H_2$]Y• in α2 should change with temperature, which would allow an estimate of their relative redox potentials. Thus, these experiments were carried out at 5, 15, 25 and 37 °C. To determine the appropriate quenching times for EPR analysis, the kinetics of $NO_2Y$• reduction in the reaction of [$NO_2Y_{122}$•]-β2/wt-α2/ATP/CDP at these temperatures were studied by SF absorption spectroscopy. In all cases, the kinetics were biphasic and the Arrhenius plot showed a linear correlation (Figure S8) suggesting that the rate determining step does not change within this temperature range. These studies also defined the timing of RFQ-EPR experiments so that quenching occurred at > 95% completion. Figure 10A shows the EPR spectra of the reactions at 5, 15, 25 and 37 °C without subtraction of the remaining $NO_2Y$• spectrum. Small changes in the EPR line shape at 3327 and 3341 G are observed (arrows, Figure 10A). These positions are close to the maximum and minimum of the simulated [β-$^2H_2$]Y• signal (Figure 9B, pink trace). Thus the observed changes indicate that increased amounts of [β-$^2H_2$]Y• are produced at higher temperatures.

The amount of [β-$^2H_2$]Y• relative to the total pathway radicals were determined as 15 ± 1, 13 ± 2, and 10 ± 2% at 37, 25 and 15 °C, respectively, using the method described above. At 5 °C, the amount of [β-$^2H_2$]Y• was too small (< 8%) for the analysis. A Δ*E*° of 110 ± 50 mV was calculated from a slope of a plot of log ([$Y_{356}$•]/[β-$^2H_2$-Y•]) vs 1/T (Figure 10B).

## Discussion

Initiation of deoxynucleotide formation with the hot oxidant $NO_2Y_{122}$•-β2, accompanied by the fortuitous uncoupling of PCET during $NO_2Y_{122}$• reduction, has allowed for the first time the observation of the three transient Y•s in the pathway (Figure 11). The inability of this RNR to turnover more than once suggests that the predominant radical, identified by our PELDOR experiments, $Y_{356}$•, is unable to reoxidize (directly or through $W_{48}$-β2) the $_{NO2}Y_{122}$ phenolate. Thus, the three Y•s observed are likely formed during the reverse PCET, subsequent to dCDP formation. These studies have confirmed the original model for this long range oxidation over 35 Å and have provided us with additional insight about the redox potentials of these three Y•s relative to one another and the radical initiator $Y_{122}$•. Furthermore the EPR analysis has provided us with insights into the H bonding environment of $Y_{356}$• and the conformations of $Y_{730}$• and $Y_{731}$•, which are essential to understanding if co-linear PCET within α2 is feasible.

### The thermodynamics of the problem

We developed three independent strategies, all using the [$NO_2Y_{122}$•]-β2 oxidant, to identify the location of Y•s and their distribution in the pathway. PELDOR experiments with wt-α2 and EPR experiments with [3,5-$F_2Y_{731(730)}$]-α2 and [β-$^2H_2$]Y-α2 together revealed that the new radical observed is a composite of three Y•s and that 85–90% of the new radical resides at $Y_{356}$ in β2 and that the remaining 10–15% is distributed equally between $Y_{731}$ and $Y_{730}$ in α2. If the observed Y•s are in equilibrium, the distribution of 9:1 at 25 °C between β2 and α2 suggests a difference in redox potential of ~70 mV. The observed temperature dependence of the amounts of these radicals, while of limited scope due to the poor sensitivity of the EPR analysis, support a redox potential difference between $Y_{356}$• and $Y_{731}$• in this range as well, 110 ± 50 mV. In addition, our EPR analysis reveals similar

amounts of 3,5-$F_2$Y• at 731 and 730-α2 indicative of small redox potential differences between these two Ys in α2. Figure 11 summarizes our current model for this process by fixing the relative redox levels of these three Ys.

Using a series of β2 mutants with $F_n$Ys replacing residue $Y_{356}$, we have previously demonstrated that dCDP production is turned off when the redox potential of $F_n$Y becomes higher than Y by 80 mV[43]. Thus $Y_{356}$ is functioning as an uphill stepping stone, likely conformationally gated, in the long range oxidation of $C_{439}$. This information starts to set the boundaries for the differences in redox potential between $Y_{122}$ and $Y_{356}$. Unfortunately spectrophotochemical methods to measure the redox potential of $Y_{122}$ have been unsuccessful. Although an estimated value of 1000 ± 100 mV has been reported[44], this number seems unlikely, as it is 100 to 200 mV higher than redox potentials of Y in peptides reported in aqueous solution.[45–48] Some recent studies from our laboratory using 2,3,5-$F_3$Y• in place of $Y_{122}$ to study nucleotide reduction, suggest that this and other $F_n$Ys at position 122 and 356 will soon allow us to bracket their differences in redox potential and the importance of conformational gating between these two Ys in β2[19].

In all the schemes describing PCET in RNR, W[48] has a prominent role (Figure 1)[3,6]. However, while it has long been established that this residue plays an essential role in electron transfer required to assemble the diferric-Y• cofactor in β2[49,50], there is currently little support[51] for its involvement in the long range radical propagation and hence we have left this residue in brackets in Figure 11. Finally, in Figure 11, we now have placed $C_{439}$ at the same redox potential as $Y_{730}$, distinct from our previous models, based on recent measurements made by Madej and Wardman[52]. If the redox potential difference between $Y_{122}$-β2 and $C_{439}$-α2 is several hundred mV, assuming an equilibrium of the radicals within the pathway, the amount of $C_{439}$• would be ~0.05 % of $Y_{122}$• at 25 °C. Given the expected rates for 2′-OH elimination of $10^{6–9}$ $s^{-1}$ [53–55], deoxynucleotide formation could still occur sufficiently fast to account for the rate of conformationally gated deoxynucleotide formation observed for wt-RNR (2–10 $s^{-1}$). Thus the overall nucleotide reduction process would be pulled to the right, by rapid, irreversible cleavage of the C2'-OH bond[56].

The first observation of pathway tyrosyl radicals has also provided mechanistically important information on the structure and environment of Ys located at the subunit interface in the active α2β2 complex. Unfortunately, atomic resolution information about the location of $Y_{356}$ relative to β2 and to $Y_{731}$ in α2 is still unavailable. EPR studies at 9 and 140 GHz and a recent crystal structure of $NH_2Y_{731}$-α2 provide additional insight about oxidation of Ys at the subunit interface.

The *g*-tensor of the Y• is only resolved by HF-EPR measurements and it has been shown that the $g_{xx}$ values are sensitive to electrostatic interactions of the protein environment and more specifically to H bonding interactions[36,57,58]. The $g_{xx}$ value for the $Y_{122}$• equivalent from RNRs of different organisms ranges from 2.0092 in *E.coli*[36] to 2.0076 in mouse[38]. High field ENDOR spectroscopy has established that the mouse Y•[58] and *S. cerevisiae* Y•[59] are H bonded. While analysis of $Y_{356}$• generated by $NO_2Y_{122}$•-β2 requires further studies by ENDOR spectroscopy to better simulate the spectra (Figure 6), the $g_{xx}$ values of 2.0063 and 2.0073 for $Y_{356}$• observed with wt-α2 and $Y_{731}$F-α2, respectively, are smaller than any previously reported $g_{xx}$ values for Y•s[35] and are likely indicative of their H bonding/ electrostatic environment. The difference between the wt and F mutant, in which a putative H bonding partner has been removed, are intriguing and require further study.

The hfc associated with one of the β-$^1$Hs of the Y•s provides insight about the Y's conformation within the active α2β2 complex and can be compared with structural data of the Y itself to learn about their mobility. For example, the $Y_{122}$•s in organisms that contain

class Ia RNRs all have similar side chain orientations ($A_{iso}$ 55 MHz)[60], while Y•s in the class Ib RNRs have similar, but distinct orientations from the Ia enzymes (Table S1). Our tentative analysis of the hfc of 3,5-$F_2Y_{731}$ gave a coupling of ~40 MHz, indicating a distinct conformation relative to that observed in wt-α2 crystal structures. This conformation would prohibit co-linear PCET between $Y_{731}$ and $Y_{730}$ in α2. We have recently reported a structure of $NH_2Y_{730}$-α2, where $Y_{731}$ in one of the three subunits in the asymmetric unit moved >9 Å from the conformation in the other subunits (Figure 8). Determination of θ from published crystallographic data for $Y_{730}$ and $Y_{731}$ reveals little variability in the case of residue 730 and much greater variability in the case of residue 731 (Table S1). Thus being able to measure the hfc at position 731 in an RNR complex is required for thinking about the mechanism of PCET at the subunit interface.

### Summary

Our observations demonstrate that Y•s trapped in the pathway reside predominantly at $Y_{356}$ in β2 with partial delocalization onto $Y_{731/730}$ in α2. This equilibrium distribution demonstrates an uphill redox gradient towards $C_{439}$ oxidation preventing accumulation of radical intermediates during long-range radical propagation. Structural information from EPR spectra at 9 and 140 GHz with several RNR variants suggests that the parallel orientation of $Y_{731}$-α2 and $Y_{730}$-α2 reported in the original X-ray structure of α2 may be different in the active α2β2 complex. These studies with combinations of unnatural amino acids site-specifically incorporated into each subunit of RNR are allowing us to understand in greater depth Nature's design principles for this unprecedented long-range oxidation.

## Supplementary Material

Refer to Web version on PubMed Central for supplementary material.

## Acknowledgments

This work was supported by NIH grants GM29595 (to J.S.), EB002804 and EB002026 (to R.G.G.). B.C. was supported by a DFG research fellowship CO802/1-1. We thank Dr. Ralph T. Weber for assistance in the PELDOR measurements.

## Reference

1. Stubbe J, van der Donk WA. Chem. Rev. 1998; 98:705–762. [PubMed: 11848913]
2. Nordlund P, Reichard P. Annu. Rev. Biochem. 2006; 75:681–706. [PubMed: 16756507]
3. Uhlin U, Eklund H. Nature. 1994; 370:533–539. [PubMed: 8052308]
4. Stubbe J, Nocera D, Yee CS, Chang MCY. Chem. Rev. 2003; 103:2167–2201. [PubMed: 12797828]
5. Yokoyama K, Uhlin U, Stubbe J. J. Am. Chem. Soc. 2010; 132:15368–15379. [PubMed: 20929229]
6. Reece SY, Hodgkiss JM, Stubbe J, Nocera DG. Phil. Trans. R. Soc. B. 2006; 361:1351–1364. [PubMed: 16873123]
7. Ge J, Yu G, Ator MA, Stubbe J. Biochemistry. 2003; 42:10071–10083. [PubMed: 12939135]
8. Ekberg M, Sahlin M, Eriksson M, Sjöberg B-M. J. Biol. Chem. 1996; 271:20655–20659. [PubMed: 8702814]
9. Climent I, Sjöberg B-M, Huang CY. Biochemistry. 1992; 31:4801–4807. [PubMed: 1591241]
10. Seyedsayamdost MR, Stubbe J. J. Am. Chem. Soc. 2006; 128:2522–2523. [PubMed: 16492021]
11. Seyedsayamdost MR, Xie J, Chan CT, Schultz PG, Stubbe J. J. Am. Chem. Soc. 2007; 129:15060–15071. [PubMed: 17990884]
12. Bennati M, Robblee JH, Mugnaini V, Stubbe J, Freed JH, Borbat P. J. Am. Chem. Soc. 2005; 127:15014–15015. [PubMed: 16248626]

13. Wang J, Lohman GJ, Stubbe J. Proc. Natl. Acad. Sci. U. S. A. 2007; 104:14324–14329. [PubMed: 17726094]
14. Schiemann O, Prisner TF. Q Rev Biophys. 2007; 40:1–53. [PubMed: 17565764]
15. Seyedsayamdost MR, Chan CT, Mugnaini V, Stubbe J, Bennati M. J. Am. Chem. Soc. 2007; 129:15748–15749. [PubMed: 18047343]
16. Bennati M, Weber A, Antonic J, Perlstein DL, Robblee J, Stubbe J. J. Am. Chem. Soc. 2003; 125:14988–14989. [PubMed: 14653724]
17. Seyedsayamdost MR, Reece SY, Nocera DG, Stubbe J. J. Am. Chem. Soc. 2006; 128:1569–1579. [PubMed: 16448128]
18. Salowe SP, Ator MA, Stubbe J. Biochemistry. 1987; 26:3408–3416. [PubMed: 3307907]
19. Minnihan EC, Young D, Stubbe J, Schultz PG. J. Am. Chem. Soc. in press.
20. Yokoyama K, Uhlin U, Stubbe J. J. Am. Chem. Soc. 2010; 132:8385–8397. [PubMed: 20518462]
21. Thelander L. J. Biol. Chem. 1973; 248:4591–4601. [PubMed: 4578086]
22. Atkin CL, Thelander L, Reichard P, Lang G. J. Biol. Chem. 1973; 248:7464–7472. [PubMed: 4355582]
23. Pannier M, Veit S, Godt A, Jeschke G, Spiess HW. J. Magn. Reson. 2000; 142:331–340. [PubMed: 10648151]
24. Jeschke G, Chechik V, Ionita P, Godt A, Zimmermann H, Banham J, Timmel CR, Hilger D, Jung H. Appl. Magn. Reson. 2006; 30:473–498.
25. Chiang YW, Borbat PP, Freed JH. J. Magn. Reson. 2005; 172:279–295. [PubMed: 15649755]
26. Becerra LR, Gerfen GJ, Bellew BF, Bryant JA, Hall DA, Inati SJ, Weber RT, Un S, Prisner TF, McDermott AE, Fishbein KW, Kreischer KE, Temkin RJ, Singel DJ, Griffin RG. J. Magn. Reson. 1995; 117:28–40.
27. Bennati M, Farrar CT, Bryant JA, Inati SJ, Weis V, Gerfen GJ, Riggs-Gelasco P, Stubbe J, Griffin RG. J. Magn. Reson. 1999; 138:232–243. [PubMed: 10341127]
28. Hahn EL. Phys Rev. 1950; 80:580–594.
29. Palmer G. Methods Enzymol. 1967; 10:595.
30. Stoll S, Schweiger A. J. Magn. Reson. 2006; 178:42–55. [PubMed: 16188474]
31. Baudot A, Alger L, Boutron P. Cryobiology. 2000; 40:151–158. [PubMed: 10788314]
32. Biglino D, Schmidt PP, Reijerse EJ, Lubitz W. Phys Chem Chem Phys. 2006; 8:58–62. [PubMed: 16482244]
33. The relative ratio of the 30 and 33 Å peaks changed upon introduction of the Y731F mutation (compare Figures 5D and 5H). The significance of this observation is currently unknown as multiple factors, such as the fitting quality and the relaxation properties of the radicals, could affect the ratio of the peaks.
34. Seyedsayamdost MR, Argirević T, Minnihan EC, Stubbe J, Bennati M. J. Am. Chem. Soc. 2009; 131:15729–15738. [PubMed: 19821570]
35. Svistunenko DA, Cooper CE. Biophysical Journal. 2004; 87:582–595. [PubMed: 15240491]
36. Gerfen GJ, Bellew BF, Un S, Bollinger JM, Stubbe J, Griffin RG, Singe DJ. J. Am. Chem. Soc. 1993; 115:6420–6421.
37. Tommos C, Tang X-S, Wamcke K, Hoganson CW, Styring S, McCracken J, Diner BA, Babcock GT. J. Am. Chem. Soc. 1995; 117:10325–10335.
38. Schmidt PP, Andersson KK, Barra AL, Thelander L, Gräslund A. J Biol Chem. 1996; 271:23615–23618. [PubMed: 8798575]
39. Unfortunately, the signals associated with the $F_2Y•$ are not sufficiently intense to allow successful PELDOR experiments.
40. Fessenden RW, Schuler RH. J. Chem. Phys. 1963; 39:2147–2195.
41. Eriksson M, Uhlin U, Ramaswamy S, Ekberg M, Regnstrom K, Sjöberg B-M, Eklund H. Structure. 1997; 5:1077–1092. [PubMed: 9309223]
42. Minnihan EC, Seyedsayamdost MR, Uhlin U, Stubbe J. J Am Chem Soc. 2011; 133:9430–9440. [PubMed: 21612216]

43. Seyedsayamdost MR, Yee CS, Reece SY, Nocera DG, Stubbe J. J. Am. Chem. Soc. 2006; 128:1562–1568. [PubMed: 16448127]
44. Silva KE, Elgren TE, Que L Jr, Stankovich MT. Biochemistry. 1995; 34:14093–14103. [PubMed: 7578006]
45. Yee CS, Seyedsayamdost MR, Chang MC, Nocera DG, Stubbe J. Biochemistry. 2003; 42:14541–14552. [PubMed: 14661967]
46. Tommos C, Skalicky JJ, Pilloud DL, Wand AJ, Dutton PL. Biochemistry. 1999; 38:9495–9507. [PubMed: 10413527]
47. DeFelippis MR, Murthy CP, Broitman F, Weinraub D, Faraggi M, Klapper MH. J. Phys. Chem. 1991; 95:3416–3419.
48. We have been using 0.83 V for the Ep of Y at pH 7.0 based on ref 46 and our independent measurement. Pulse radiolysis methods, however, report a value of 0.93 V, as in ref 47 and references therein.
49. Baldwin J, Krebs C, Ley BA, Edmondson DE, Huynh BH, Bollinger JM. J. Am. Chem. Soc. 2000; 122:12195–12206.
50. Bollinger JM, Tong WH, Ravi N, Huynh BH, Edmonson DE, Stubbe J. J. Am. Chem. Soc. 1994; 116:8024–8032.
51. Rova U, Goodtzova K, Ingemarson R, Behravan G, Gräslund A, Thelander L. Biochemistry. 1995; 34:4267–4275. [PubMed: 7703240]
52. Madej E, Wardman P. Arch Biochem Biophys. 2007; 462:94–102. [PubMed: 17466930]
53. Steenken S, Davies MJ, Gilbert BC. J. Chem. Soc. Perkin Trans. 2. 1986:1003–1010.
54. Bansal KM, Grätzel M, Henglein A, Janata E. J. Phys. Chem. 1973; 77:16–19.
55. Lenz R, Giese B. J. Am. Chem. Soc. 1997; 119:2784–2794.
56. Licht S, Stubbe J. Comprehensive Natural Product Chemistry. 1999; 5:163–203.
57. Hoganson CW, Babcock GT. Biochemistry. 1992; 31:11874–11880. [PubMed: 1332777]
58. van Dam PJ, Willems J-P, Schmidt PP, Pötsch P, Barra AL, Hagen WR, Hoffman BM, Andersson KK, Gräslund A. J. Am. Chem. Soc. 1998; 120:5080–5085.
59. Bar G, Bennati M, Nguyen HH, Ge J, Stubbe JA, Griffin RG. J. Am. Chem. Soc. 2001; 123:3569–3576. [PubMed: 11472128]
60. Lendzian F. Biochim. Biophys. Acta. 2005; 1707:67–90. [PubMed: 15721607]
61. Högbom M, Andersson ME, Nordlund P. J. Biol. Inorg. Chem. 2001; 6:315–323. [PubMed: 11315567]

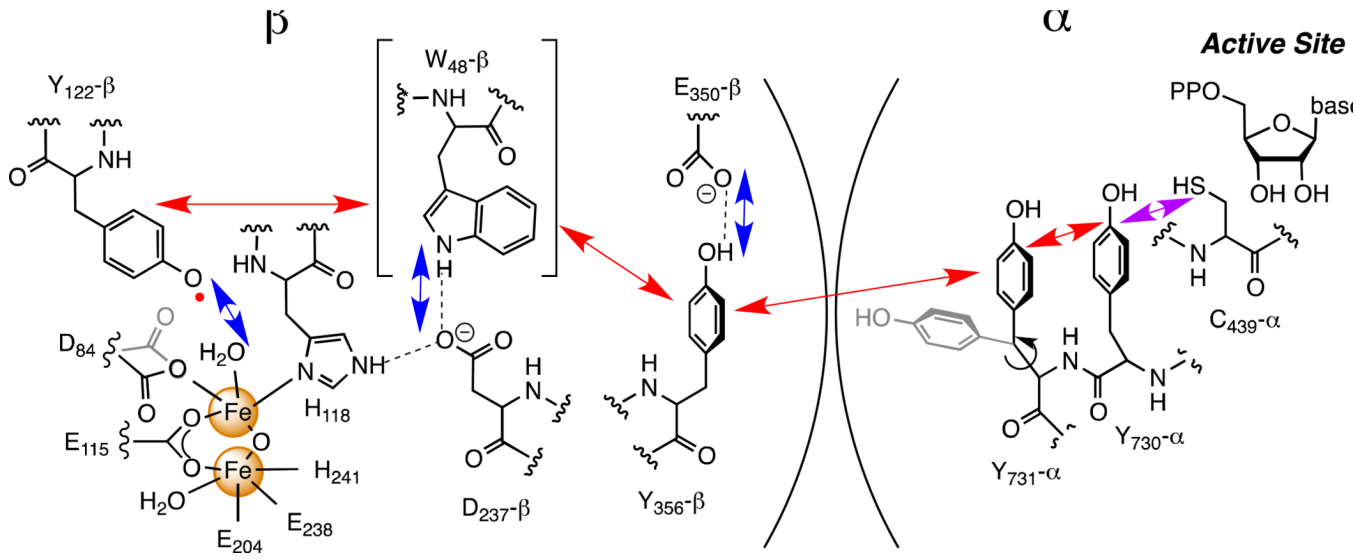


**Figure 1.**

Proposed PCET pathway in *E. coli* class Ia RNR. Alternative conformations found in crystal structures are shown in gray for $D_{84}$-β2 (PDB ID, 1JQC[61]) and $Y_{731}$-α2 (PDB ID, 2XO4[42]). Red and blue arrows indicate orthogonal transfer of an electron and proton, respectively. The proton acceptor for $Y_{731}$-α2 during its transient oxidation is unknown. The purple arrow in α2 indicates co-linear movement of the electron and proton. $Y_{356}$- and $E_{350}$-β2 are in the flexible C-terminal tail and are disordered in all crystal structures. There is currently no direct evidence for the involvement of $W_{48}$-β2 in the radical propagation process, hence indicated by [ ].

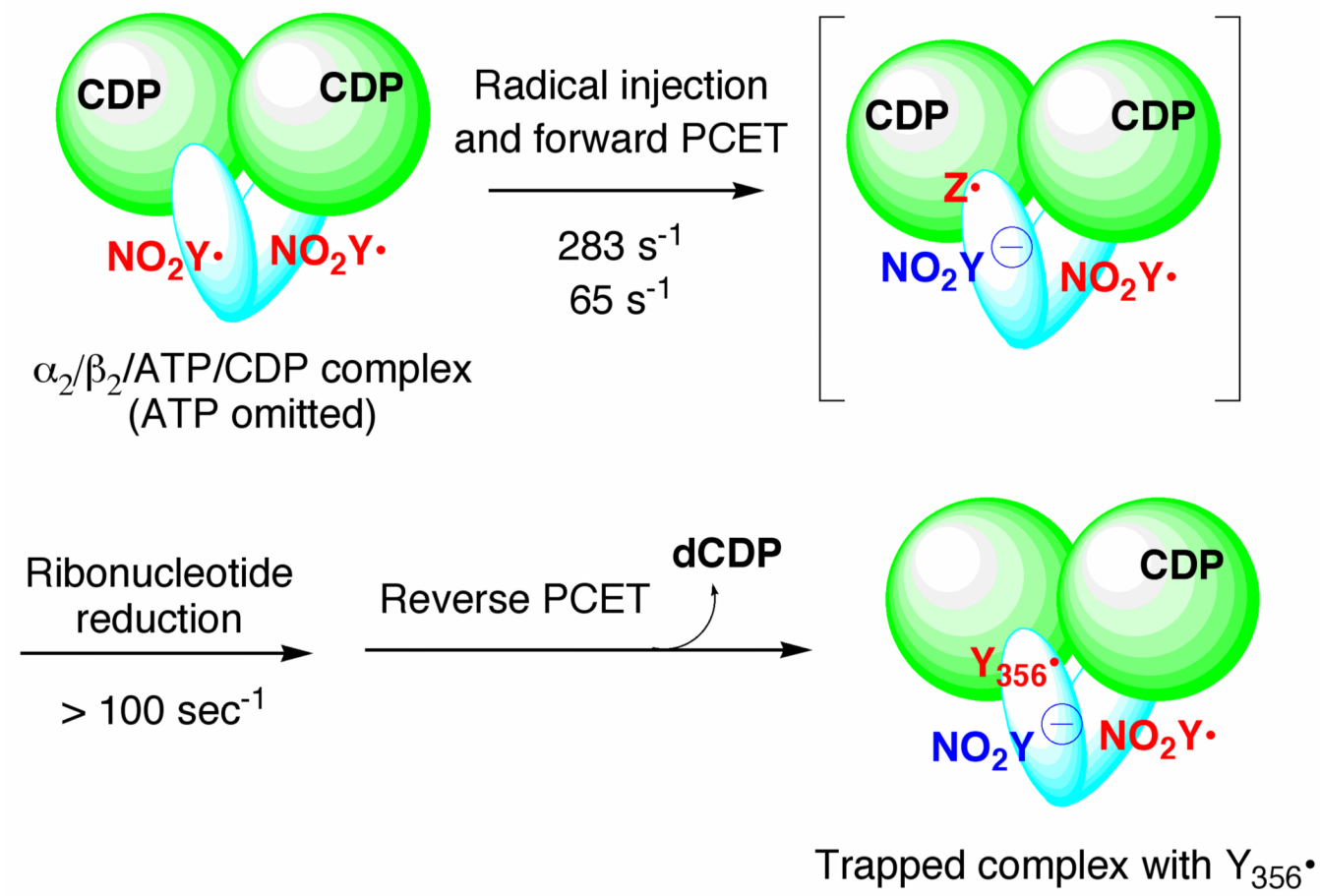


**Figure 2.**

Model for the reaction of [$NO_2Y_{122}$•]-β2 with α2, ATP, and CDP based on rapid kinetics experiments[5]. The green circles represent α, and the blue ovals, β. ATP, the allosteric effector, is omitted from α for clarity. There are 1.2 $NO_2Y$•/β2, not two as shown in the figure and their distribution between the two monomers of β is not understood. Any intermediate(s) between the forward PCET and ribonucleotide reduction is (are) designated as Z•. Rate constants determined for dCDP and Y• formation (> 100 $s^{-1}$) are limited by the time resolution of the instrument measurement and these steps likely exhibit biphasic kinetics with rate constants similar to the $NO_2Y$ phenolate formation.

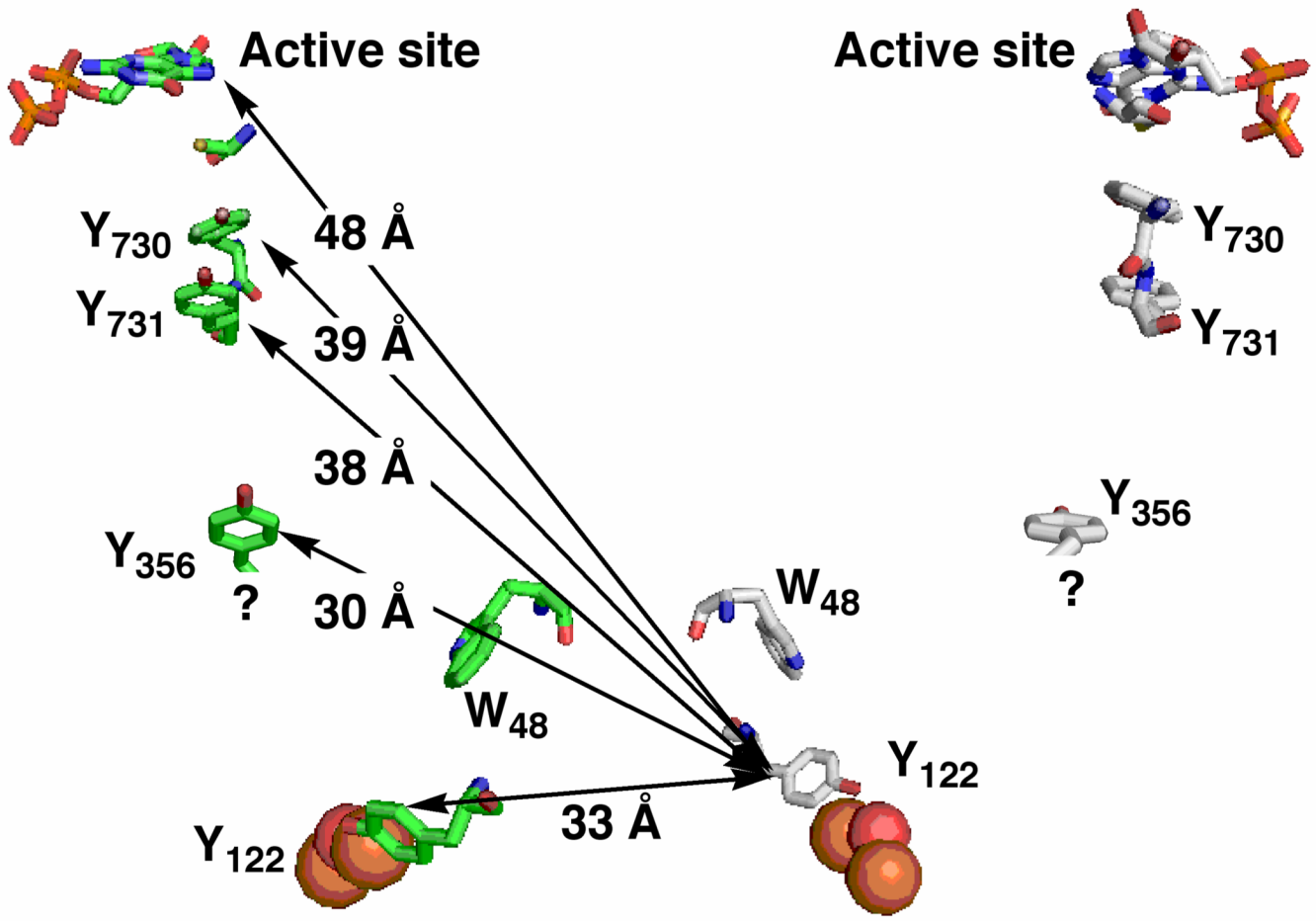


**Figure 3.**

Diagonal distances previously measured in wt and mutant RNRs by PELDOR spectroscopy. Distances shown were determined by PELDOR for $Y_{122}$•/$Y_{122}$• (33 Å)[16], $Y_{122}$•/DOPA$_{356}$• (30 Å)[15], $Y_{122}$•/$NH_2Y_{731}$• (38 Å)[15], $Y_{122}$•/$NH_2Y_{730}$• (39 Å)[15], and $Y_{122}$•/N• (48 Å, N• is a nitrogen centered radical observed in the reaction with a mechanism based inhibitor, 2′-azido-2′-deoxynucleotide diphosphate)[12]. The residues constituting a pathway in one αβ pair are colored in green, and the residues in the second pathway are shown in grey. $Y_{356}$-β2 is disordered in all crystal structures.

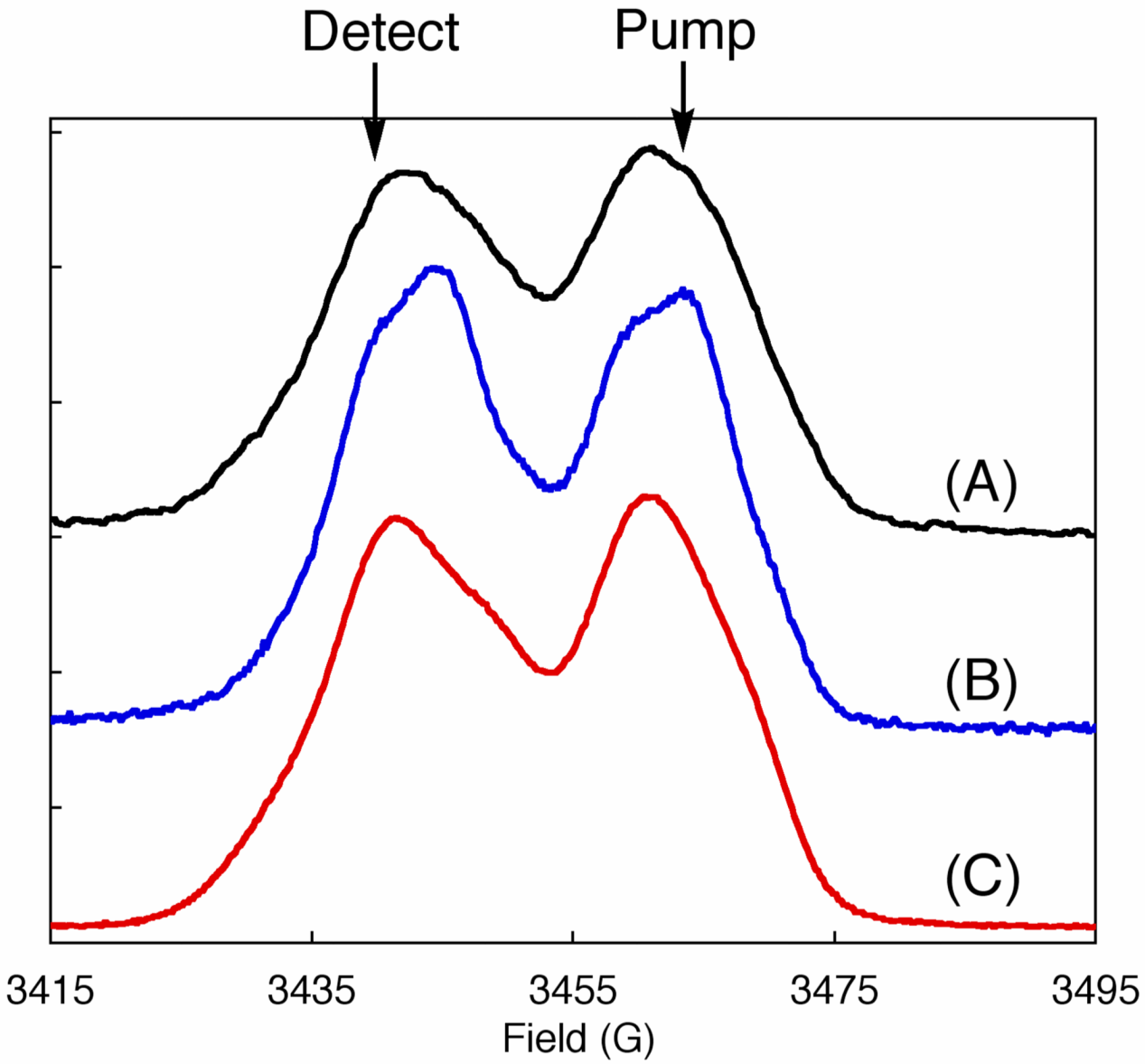


**Figure 4.**

Spin-echo detected 9 GHz EPR spectrum of the reaction of [$NO_2Y_{122}$•]-β2 with α2/ATP/CDP rapid freeze quenched at 24 ms and recorded at 5 K (A, ~34% trapped Y• and ~66% $NO_2$Y•) and at 80 K (B, only trapped Y• is observable). C. Absorption spectrum of [$NO_2Y_{122}$•]-β2 alone at 5 K.

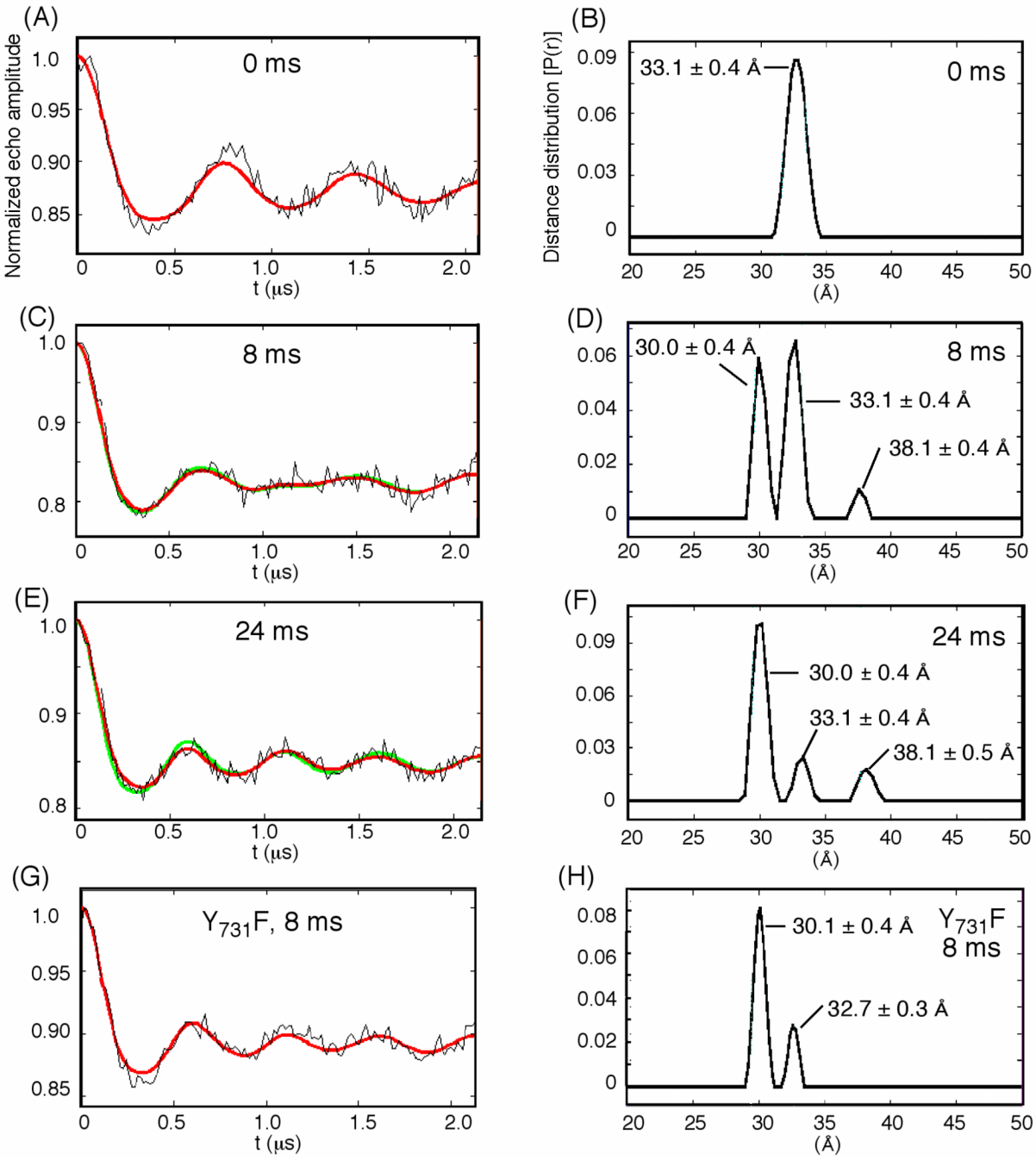


**Figure 5.**

Left column: normalized four-pulse DEER oscillations at 5 K for [$NO_2Y_{122}$•]-β2 alone (A); the [$NO_2Y_{122}$•]-β2/wt-α2/ATP/CDP reaction freeze quenched at 8 ms (C) and 24 ms (E); the [$NO_2Y_{122}$•]-β2/$Y_{731}$F-α2/ATP/CDP reaction freeze quenched at 8 ms (G). The overlaid red lines are fits using the Tikhonov regularization procedure[25]. Green lines in (C) and (E) are fits without the 38 Å feature. Right column: distance distributions obtained from the analysis of the spectra in the left column. While the relative populations of the 30 and 33 Å peaks changed when $Y_{731}$ was replaced with F, its significance is currently unknown as multiple factors, such as the fitting quality and the relaxation properties of the radicals, might contribute to the altered ratio.

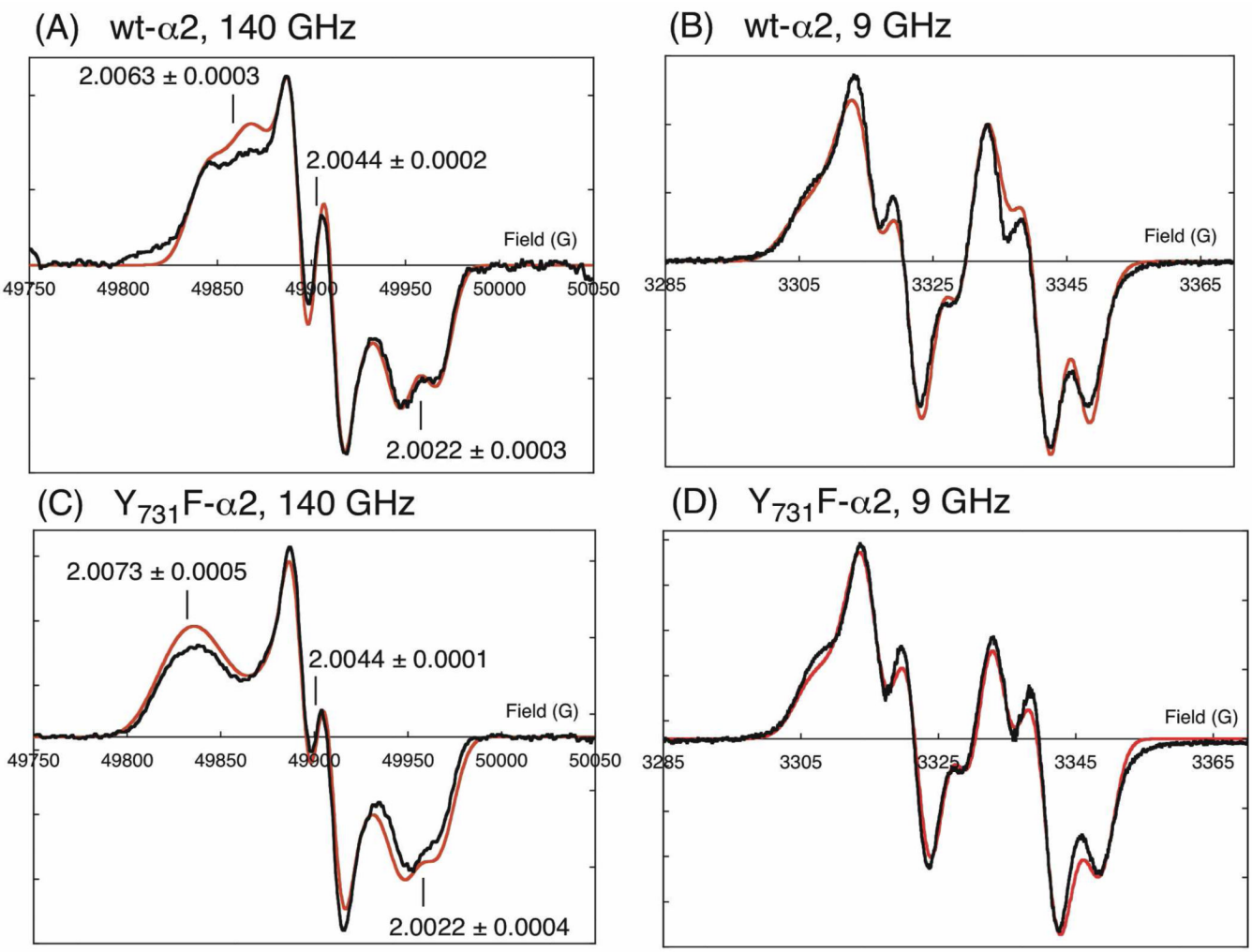


**Figure 6.**

EPR spectra at 140 GHz and 9 GHz of pathway Y•s observed in the wt-α2 and $Y_{731}$F-α2 reactions. The reactions were carried out at room temperature with 170 μM wt or $Y_{731}$F-α2, 170 μM [$NO_2Y_{122}$•]-β2, 3 mM ATP and 1 mM CDP, and freeze-quenched in the cryostat after ~15 s. The 140 GHz and 9 GHz spectra for each reaction were simulated (red traces) using the same set of parameters (Table 1) as described in the text. The g-values determined by the simulation are indicated in (A) and (C).

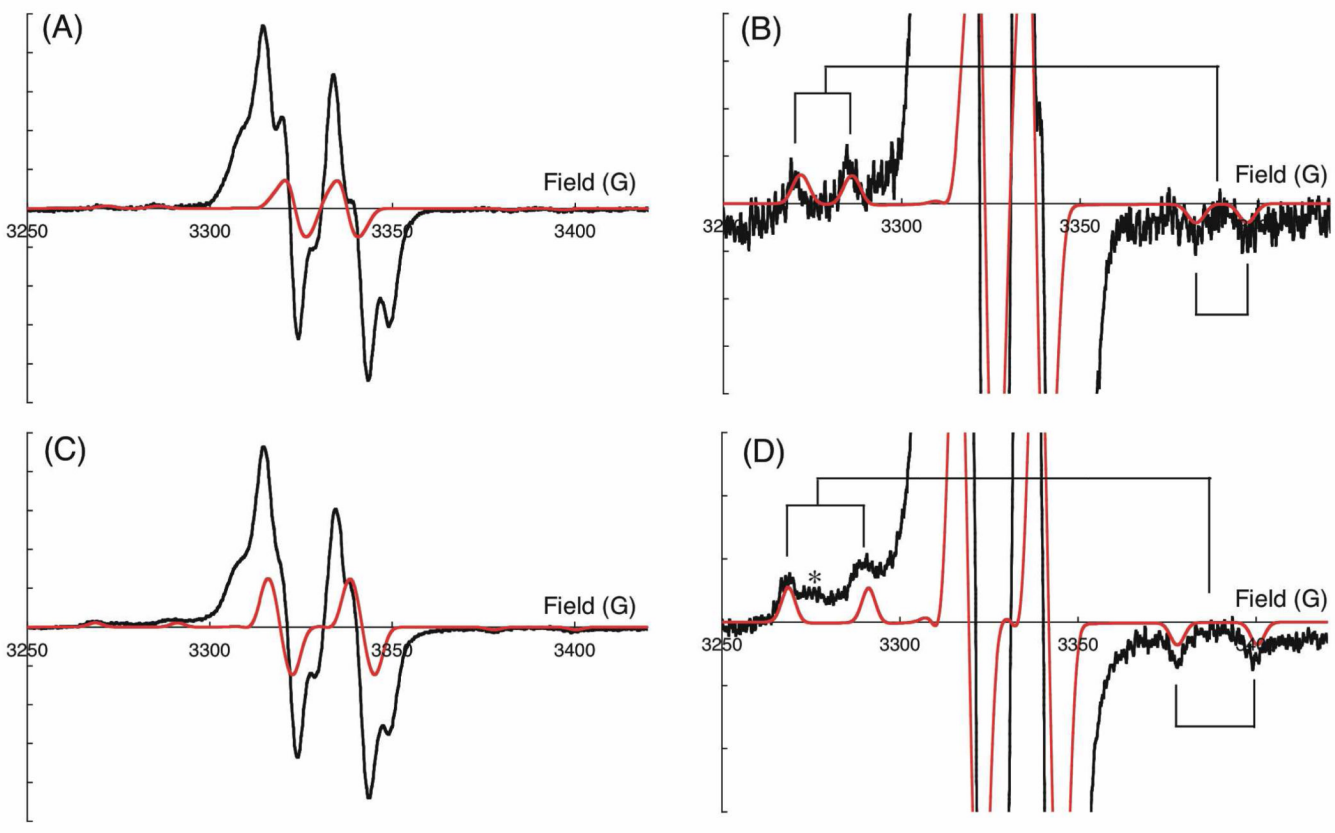


**Figure 7.**

EPR spectra of the pathway radicals formed in the reaction of [3,5-$F_2Y_{731}$]-α2 (A and B) or [3,5-$F_2Y_{730}$]-α2 (C and D) with [$NO_2Y_{122}$•]-β2/ATP/CDP quenched at 60 ms (black traces) overlaid with simulated EPR spectra of 3,5-$F_2Y$• (red traces). The EPR spectrum of $NO_2Y$• (50% of total radical) was subtracted from the observed spectrum. (B) and (D) are a magnified view of (A) and (C), respectively. The EPR spectral simulations were carried out using the parameters shown in Table 1. Only the low and high-field doublet features were simulated as described in the text. * in (D) indicates an uncharacterized signal that has also been observed in the reaction with wt-α2. Brackets in (B) and (D) indicate the hyperfine splitting associated with $^{19}F$ and β-$^{1}H$.

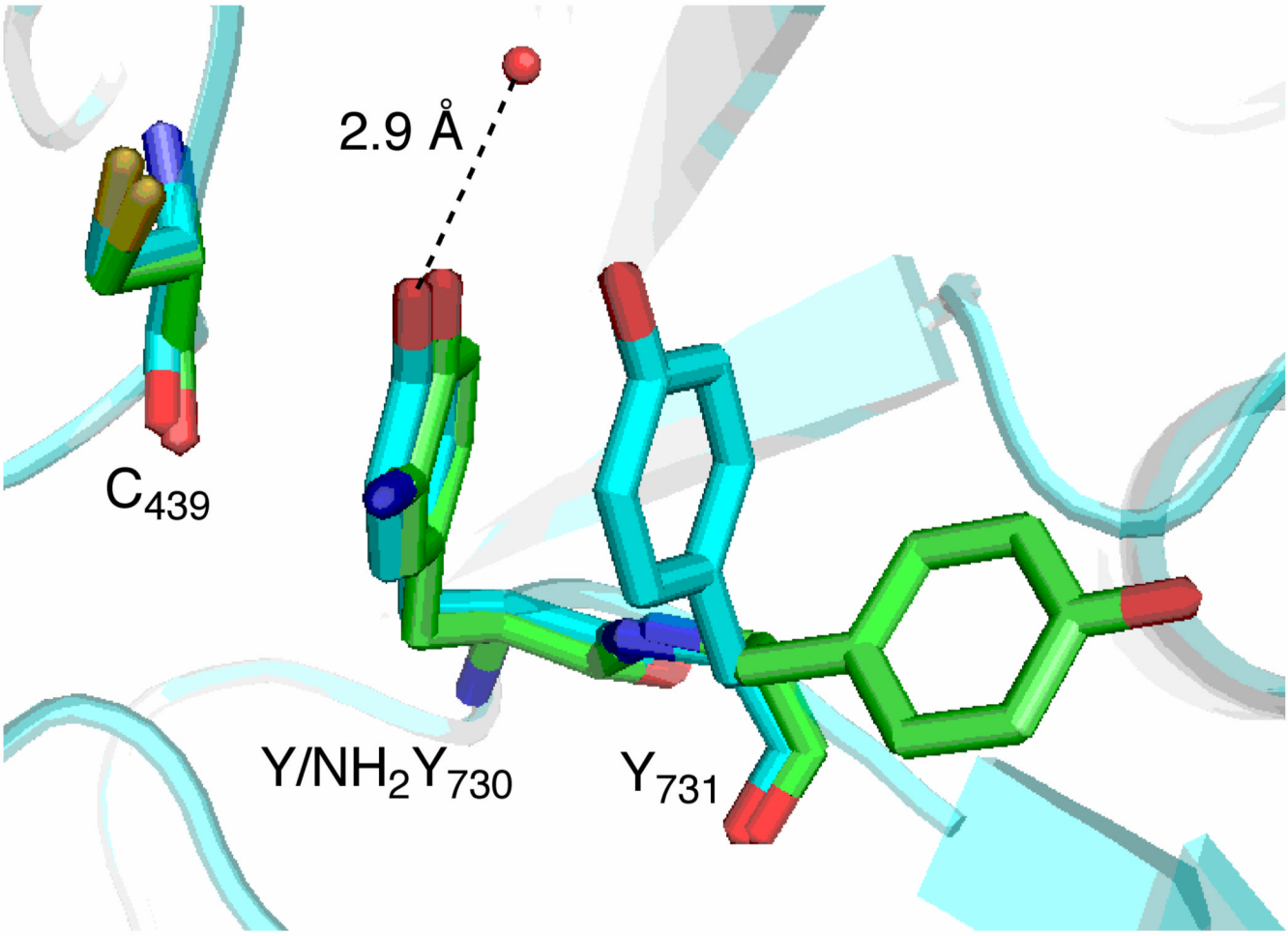


**Figure 8.**
Overlay of X-ray structures of pathway residues in wt-α2 (blue, PDB ID, 2X0X)[20] and in one of the three subunits in the asymmetric unit of the crystal structure of [$NH_2Y_{730}$]-α2 (green, PDB ID, 2XO4)[42]. A conserved water molecule close to the 730 residue is shown along with the distance to the phenol oxygen atom of $Y_{730}$-α2.

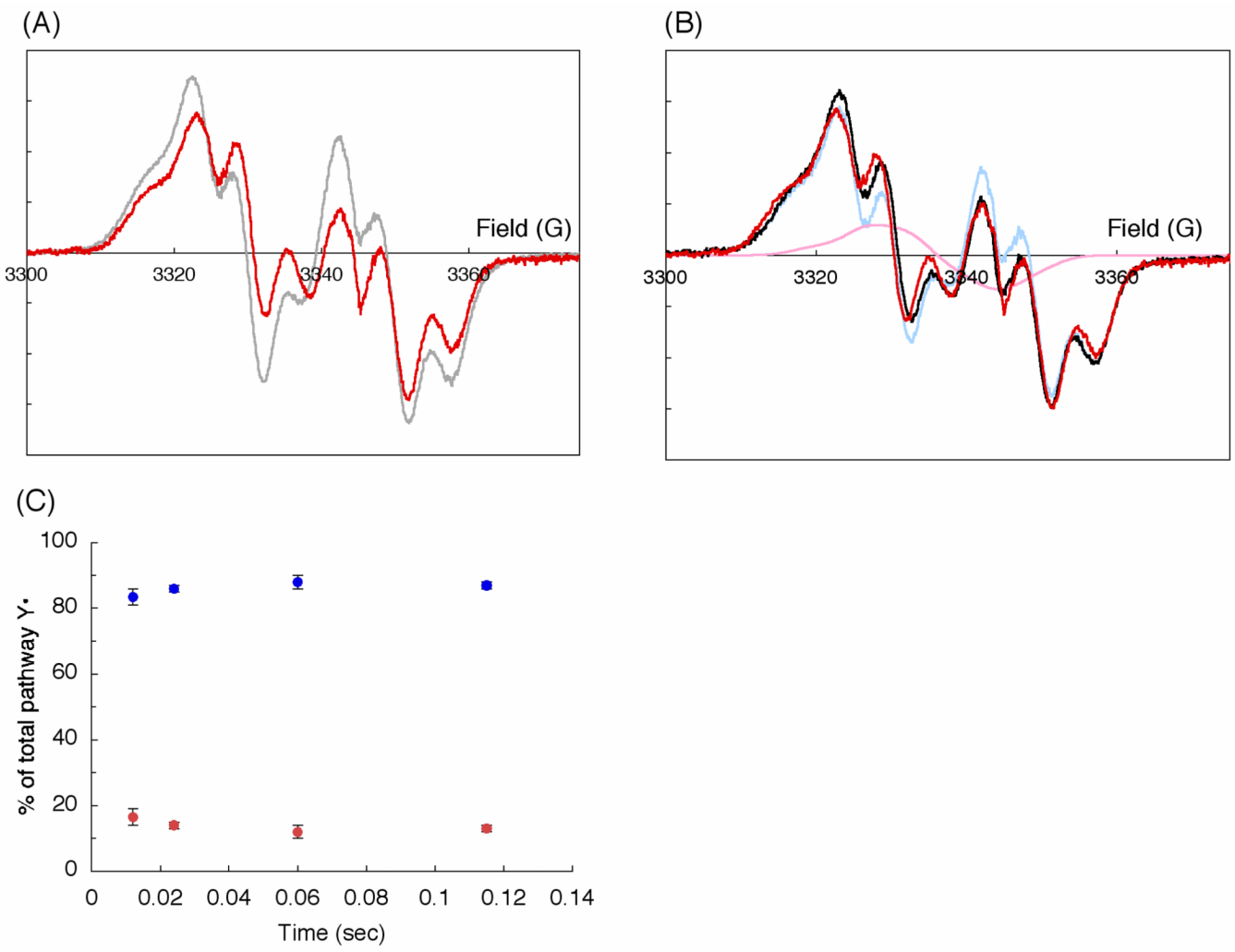


**Figure 9.**

(A) EPR spectrum of pathway Y•s observed in the reaction with [$NO_2Y_{122}$•]-β2/[β-$^2H_2$]Y-α2/ATP/CDP carried out at 25 °C and quenched at 115 ms (red trace). The EPR spectrum observed in the same reaction using non-labeled α2 is overlaid (gray trace). The $NO_2Y_{122}$• spectrum (50% of the total radical) was subtracted from the observed spectra in both cases. (B) EPR spectral reconstruction using the spectrum of $Y_{356}$• observed in the [$NO_2Y_{122}$•]-β2/[$Y_{731}$F]-α2/ATP/CDP reaction (blue, 87%) and that of [β-$^2H_2$]Y• simulated using the parameters shown in Table 1 as described in the text (pink, 13%). The sum of the two spectra is shown in the black trace and overlaid with the EPR spectrum of pathway Y•s observed in the [$NO_2$ $Y_{122}$•]-β2/[β-$^2H_2$]Y-α2/ATP/CDP reaction freeze quenched at 115 ms (red trace). (C) Timecourse of the relative ratios of $Y_{356}$• (blue) and [β-$^2H_2$]Y• (red) at 25 °C determined as described in (B). Each point represents an average of two or three experiments.

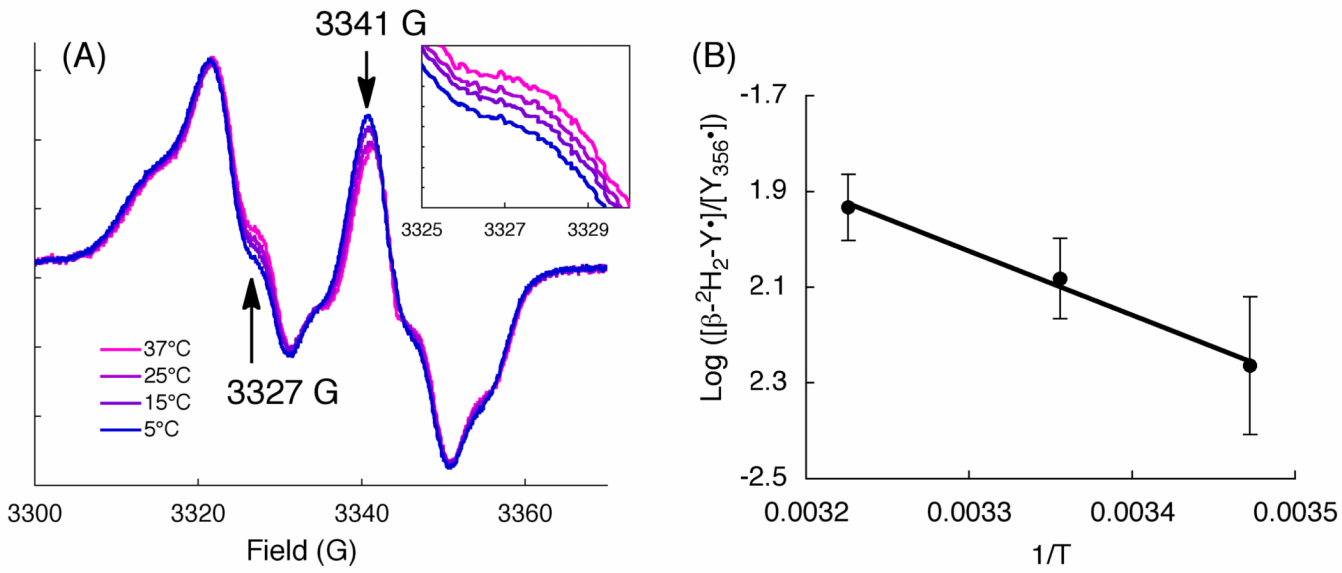


**Figure 10.**

(A) Overlaid EPR spectra of the [$NO_2Y_{122}$•]-β2/[β-$^2H_2$]Y-α2/ATP/CDP reaction at 5 (blue), 15, 25 and 37 °C (red) without subtraction of the $NO_2Y$• spectrum. The arrows indicate the change induced by the shift in the temperature. Each spectrum is an average of two or three experiments. Inset is a magnified view between 3325 and 3330 G. (B) A plot of log ([β-$^2H_2$-Y•]/[$Y_{356}$•]) vs 1/T. The [β-$^2H_2$-Y•] determined for the reactions at 15, 25, and 37°C were used. At 5 °C, the amount of [β-$^2H_2$]Y• could not be quantitated. The line is a linear least square fit to Eq. 1 with $\Delta E°$ = 110 mV. Each point represents an average of two or three experiments.

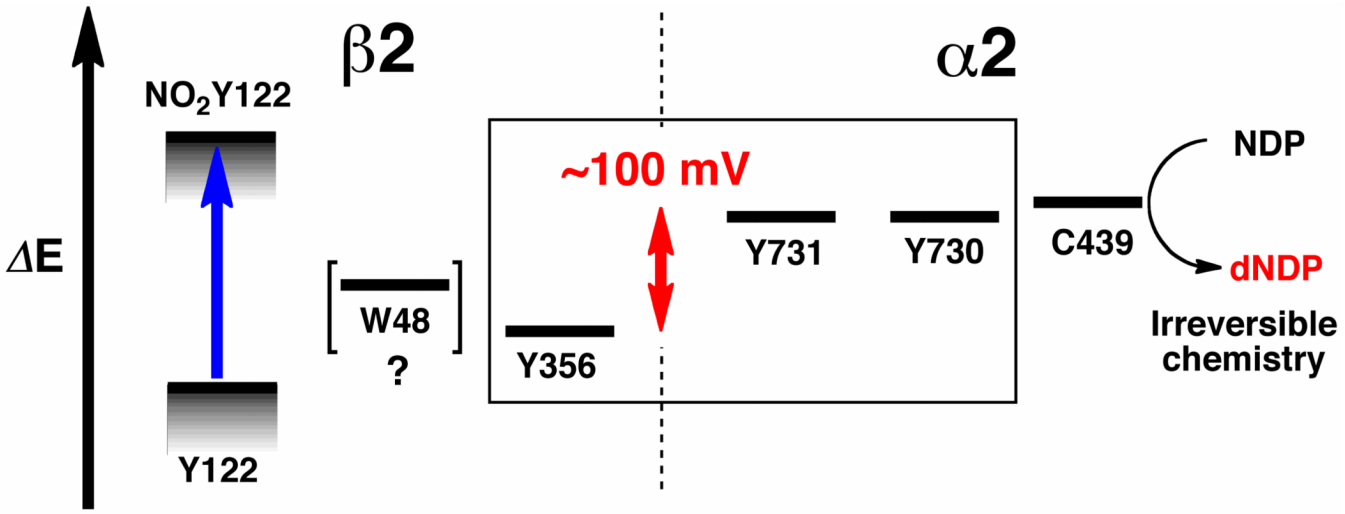


**Figure 11.**

A model of the relative redox potentials of PCET pathway residues in *E. coli* RNR. The box highlights $Y_{356}$-β2, $Y_{731}$- and $Y_{730}$-α2, the Y•s observed in the present studies. $W_{48}$-β2 is in brackets as there is currently no direct evidence for its involvement in the radical propagation process. The range of the redox potential for $NO_2Y_{122}$, which in solution at pH 7.0 is 210 mV[45] harder to oxidize than Y, is based on the unknown redox potential for $Y_{122}$, hence the shaded area. The placement of $Y_{356}$ relative to $Y_{122}$ is based on studies with 2,3,5-$F_3Y_{122}$• (+20 ~ +100 mV harder to oxidize than Y between pH 6.5 – 8.0, assuming no p$K_a$ perturbation by the protein) as the radical initiator where the $Y_{356}$• is detected[19].

**Table 1**

Hfcs (in MHz) used in the EPR simulations.

| Position | Nucleus | $A_{xx}$ | $A_{yy}$ | $A_{zz}$ |
|---|---|---|---|---|
| 3,5-$F_2Y_{730}$•[a,b] | β-$^1$H[e,f] | 63 | 63 | 63 |
| | $^{19}F_a$[e,g] | −15 | −3 | 151 |
| | $^{19}F_b$[e,g] | 15 | 3 | −151 |
| 3,5-$F_2Y_{731}$•[a,b] | β-$^1$H[e,f] | 40 | 40 | 40 |
| | $^{19}F_a$[e,g] | −15 | −3 | 157 |
| | $^{19}F_b$[e,g] | 15 | 3 | −157 |
| [β-$^2H_2$]Y•[a,b] | 3,5-$^1$H[h] | 27 | 8 | 19 |
| | β-$^2$H[e,f] | 8 | 8 | 8 |
| Pathway Y• in the wt-α2 reaction[a,c] | 3,5-$^1$H[h] | 26 | 4 | 18 |
| | β-$^1$H[e] | 61 | 52 | 54 |
| Pathway Y• in the $Y_{731}$F-α2 reaction[a,d] | 3,5-$^1$H[h] | 26 | 4 | 18 |
| | β-$^1$H[e] | 54 | 52 | 54 |

[a] The intrinsic EPR linewidth of 17 MHz was used. Hfcs for 2,6-$^1$H and one of the two β-$^1$Hs or β-$^2$Hs were not included in the simulation as they are significantly smaller than the intrinsic EPR linewidth.

[b] g-values of 2.0063, 2.0044, and 2.0022 were used based on the assumptions described in the text.

[c] g-values of 2.0063, 2.0044 and 2.0022 were used.

[d] g-values of 2.0073, 2.0044 and 2.0022 were used.

[e] Hyperfine tensor axes were assumed to be co-linear with the *g* tensor axes[17,35].

[f] Hfcs for β-$^1$H or β-$^2$H were assumed isotropic based on the reported small anisotropy for this position[35].

[g] $A_{xx}$ and $A_{yy}$ for $^{19}$F were chosen based on the previous characterization of 3-FY•[17].

[h] The Euler angles of [α, β, γ] = [±22°, 0°, 0°][35] were used.